

EFFECTS OF A ROGUE STAR ON EARTH'S CLIMATE

A DISSERTATION

SUBMITTED TO THE FACULTY OF THE GRADUATE SCHOOL  
OF THE UNIVERSITY OF MINNESOTA

BY

HARINI CHANDRAMOULI

IN PARTIAL FULFILLMENT OF THE REQUIREMENTS  
FOR THE DEGREE OF  
DOCTOR OF PHILOSOPHY

RICHARD McGehee

AUGUST 2020

© HARINI CHANDRAMOULI 2020  
ALL RIGHTS RESERVED

# Acknowledgements

I would like to express my gratitude to the following people without whom I would not be where I am today:

Dick McGehee, who has been the best advisor I could have asked for. His guidance, kindness, strength, and unrelenting patience has taught me what it means to be a good teacher and to never stop fighting for what I want. Bonny Flemming, who is always willing to lend an ear and making sure that all that paperwork got submitted correctly. Bryan Mosher, for letting me flex my teaching muscles and all the mentoring you've given me over the years. Rick Moeckel, Clarence Lehman, and Paul Garrett, for serving on my committee and making my dissertation a smooth process, even in the face of all that 2020 had to throw at us. Arnd Scheel and Gareth Roberts, for taking the time to write me letters of recommendation and helping me write and speak about my own mathematics better. David Swigon, for encouraging me to do mathematical research and being the first person to ever tell me that I should go to graduate school.

To my many friends who have been with me throughout this journey, I cannot thank you enough. Sunita Chepuri, for always being by my side (literally). I couldn't have done this without you. Cora Brown and Sarah Milstein, for listening to my endless babble and making me feel like I belonged in the world of mathematics. Alice Nadeau, for being my graduate school inspiration and pushing me to strive for more. My academic twin, Somyi Baek, for spending this last year helping me to stay motivated. Daniel

Hess, for giving me confidence when I had none and comfort when I needed it the most. Jimmy Broomfield, Greg Michel, and Mike Loper, for helping to create best cohort that the School of Mathematics has ever seen. My office mates past and present (Sunita Chepuri, Cora Brown, Becky Patrias,Carolynn Johnson, Olivia Cannon, Emily Tibor, and Dario Valdebenito), who have made Vincent Hall 552 to most enviable office in the whole department. Therese Broomfield, Rachel Johnson, Maclane Marti, and Brian Barthel, who have helped make Minnesota my home.

Finally, to my family whose support has seen me through numerous crises. Amma, Appa, Anna, and Kendra, for always making time for me and helping me to keep everything in perspective. Anand and Veera, for always providing me with the best baby content to brighten up my many difficult days.

# Dedication

For giving me opportunities they never had and for their unwavering support, this work is dedicated to my parents, Kodaganallur Shankaranarayanan Chandramouli and Latha Chandramouli.

## Abstract

The details of the way in which the Earth orbits the Sun can have profound effects on Earth's climate. Elements such as the Earth's tilt or how tight the orbit is can affect temperature distribution or glacial formation. One event that could lead to such changes is if a star passes near our solar system close enough to disturb Earth's orbit. Over the Earth's 4.5 billion year history, many stars could have approached the Solar System. Disturbances that are forced due to such an event could have effects on the orbit of planets in the Solar System. Even small changes to the orbits of the planets can have large effects on the climate a planet experiences as they could disrupt the Milankovitch cycles. These effects would be visible in the Earth's sediment core data, which can be used to help model the Earth's position as it orbits the Sun.

This work focuses on modeling the effects of a star passing within the Solar System on the eccentricity, semi-major axis, and argument of the periapsis. The changes to the Earth's climate due to the changes on those orbital elements are also considered. Here the focus is on what the system would look like if the star were to pass within Kuiper Belt and the Oort Cloud. Passage within the Kuiper Belt has can change the equilibrium temperature of the Earth up to  $2^{\circ}$  C without even taking into consideration the interactions of the planets with each other on the climate. The position of a planet as the star passes has an effect on the system, giving different results for different initial conditions. This position is seen to lead to dramatic differences between the orbital elements for various solutions.

# Contents

<b>Acknowledgements</b>	<b>i</b>
<b>Dedication</b>	<b>iii</b>
<b>Abstract</b>	<b>iv</b>
<b>List of Tables</b>	<b>viii</b>
<b>List of Figures</b>	<b>xi</b>
<b>1 Introduction</b>	<b>1</b>
<b>2 The Hyperbolic Restricted Three-Body Problem</b>	<b>5</b>
2.1 Conserved Quantities, Symmetries, and Integrals of Motion . . . . .	8
2.2 Relative Coordinate System . . . . .	10
2.2.1 Regularization Methods . . . . .	12
2.3 Other Work on the HR3BP . . . . .	15
2.3.1 Approach by Faintich . . . . .	16
2.3.2 Approach by Sorokovich . . . . .	17
2.4 Discussion . . . . .	19

<b>3</b>	<b>Energy Balance Models</b>	<b>20</b>
3.1	Description of the Model . . . . .	21
3.1.1	Absorbed Solar Radiation . . . . .	22
3.1.2	Outgoing Radiation . . . . .	24
3.1.3	Transport . . . . .	25
3.1.4	Dynamic Ice Line . . . . .	25
3.1.5	Values of Parameters in the Budyko Model . . . . .	26
3.2	Effects of the Semi-Major Axis and Eccentricity on Temperature Distribution . . . . .	26
3.3	Discussion . . . . .	29
<b>4</b>	<b>Passage in the Kuiper Belt</b>	<b>30</b>
4.1	Initial Conditions . . . . .	33
4.1.1	Values of Parameters in Simulations . . . . .	35
4.2	Effects on the Orbit of Jupiter . . . . .	35
4.3	Effects on the Orbit and Climate of Earth . . . . .	43
4.3.1	Global Mean Temperature Changes . . . . .	49
4.3.2	Equilibrium Temperature Profile Changes . . . . .	50
4.3.3	Bifurcation Diagram in the Semi-Major Axis . . . . .	53
4.4	Discussion . . . . .	55
<b>5</b>	<b>Passage near the Oort Cloud</b>	<b>57</b>
5.1	Varying Star's Distance with Constant Initial Position of the Planet . . . . .	58
5.1.1	Global Mean Temperature Changes . . . . .	62
5.1.2	Equilibrium Temperature Profile Changes . . . . .	65
5.2	Varying the Initial Position of the Planet . . . . .	65
5.2.1	Global Mean Temperature Changes . . . . .	66



5.2.2	Equilibrium Temperature Profile Changes . . . . .	70
5.3	Discussion . . . . .	70
<b>6</b>	<b>Discussion</b>	<b>73</b>
6.1	Future Work . . . . .	75
	<b>References</b>	<b>76</b>
	<b>Appendix A. Mathematica Code</b>	<b>84</b>
A.1	Regularized HR3BP in 2D . . . . .	84
A.2	Budyko-Widiasih Model . . . . .	96

# List of Tables

3.1	Parameter values used in the standard Budyko-Widiasih EBM for Earth.	26
4.1	Masses of known stars that have passed or will pass within 5 light-years of the Sun within $\pm 3$ million years measured in $M_{\odot}$ , where $1 M_{\odot}$ is the mass of the Sun. . . . .	31
4.2	Initial conditions of the HR3BP for both Jupiter and Earth as the third body in an elliptic orbit and the star passing in the middle of the Kuiper Belt. The system has been scaled so that Jupiter could be a distance of 1 unit away. . . . .	37
4.3	Final value of eccentricity ( $e_J(\mathbf{smax})$ ), percentage change in the semi-major axis ( $\% \Delta a_J$ ), final value of orbital period ( $T_J(\mathbf{smax})$ ), and the final value of the argument of the periapsis ( $\omega_J(\mathbf{smax})$ ) for the simulations with initial conditions found in the first two columns, along with those found in table 4.2. Recall that the initial value of $e_J$ is 0.0489, the initial value for $a_J$ is 1, the initial value of $T_J$ is 7.82391, and the initial value of $\omega_J$ is 0 degrees. . . . .	40

4.4	Final value of eccentricity ( $e(\mathbf{smax})$ ), percentage change in the semi-major axis ( $\% \Delta a_E$ ), final value of orbital period ( $T_E(\mathbf{smax})$ ), and the final value of the argument of the periapsis ( $\omega_E(\mathbf{smax})$ ) for the simulations with initial conditions found in the first two columns, along with those found in table 4.2. Recall that the initial value of $e_E$ is 0.0167, the initial value for $a_E$ is 0.192, the initial value of $T_E$ is 0.658227, and the initial value of $\omega_E$ is 0 degrees. . . . .	46
5.1	Initial conditions of the HR3BP for Jupiter as the third body in an elliptic orbit starting on the horizontal axis. The system has been scaled so that Jupiter could be a distance of 1 unit away. . . . .	58
5.2	Final value of eccentricity ( $e_J(\mathbf{smax})$ ), percentage change in the semi-major axis ( $\% \Delta a_J$ ), final value of orbital period ( $T_J(\mathbf{smax})$ ), and final value of the argument of the periapsis ( $\omega_J(\mathbf{smax})$ ) for the simulations with distance of closest approach given by the first column, $a$ , along with those found in table 5.1. Recall that the initial value of $e_J$ is 0.0489, the initial value for $a_J$ is 1, the initial value of $T_J$ is 7.82391, and the initial value of $\omega_J$ is 0 degrees. . . . .	62
5.3	The difference between the global mean temperature (GMT) before the star passes to after the star passes at various ice line locations and for various closest approaches of the star. If the number is negative, the global mean temperature increases after the star passes, and if it is positive, the global mean temperature decreases after the star passes. . . . .	64
5.4	Orbital elements after the star passes from varying distances (closest approach of star given in column 1). The starting locations (column 2) that resulted in the largest changes in the eccentricity are given. . . . .	67

5.5	Orbital elements after the star passes from varying distances (closest approach of star given in column 1). The starting locations (column 2) that resulted in the largest changes in the semi-major axis are given. . .	67
5.6	Orbital elements after the star passes from varying distances (closest approach of star given in column 1). The starting locations (column 2) that resulted in the largest changes in the argument of the periapsis are given. . . . .	67

# List of Figures

2.1	Initial two-body problem that is present before the rogue star passes through the system. . . . .	6
2.2	Relative coordinate system transformation. . . . .	10
3.1	Sensitivity of changes in the eccentricity to changes in the semi-major axis. . . . .	28
3.2	Effects of eccentricity on the equilibrium temperature profile for Earth. . . . .	28
4.1	The initial set-up of the problem in this chapter 4 is drawn. . . . .	36
4.2	Jupiter's initial orbit and final orbit are drawn in the $(q_1, q_2)$ plane as the star passes for initial position $(1.0489, 0)$ of Jupiter. . . . .	38
4.3	Jupiter's initial orbit's and final orbit's eccentricity, semi-major axis, and argument of the periapsis values as the star passes for initial position $(1.0489, 0)$ of Jupiter. . . . .	38
4.4	Jupiter's initial orbit and final orbit are drawn in the $(q_1, q_2)$ plane as the star passes for initial position $(-0.87498, -0.382226)$ of Jupiter. . . . .	41
4.5	Jupiter's initial orbit's and final orbit's eccentricity, semi-major axis, and argument of the periapsis values as the star passes for initial position $(-0.87498, -0.382226)$ of Jupiter. . . . .	41
4.6	Jupiter's initial orbit and final orbit are drawn in the $(q_1, q_2)$ plane as the star passes for initial position $(-0.658207, -0.706261)$ of Jupiter. . . . .	42

4.7	Jupiter's initial orbit's and final orbit's eccentricity, semi-major axis, and argument of the periapsis values as the star passes for initial position $(-0.658207, -0.706261)$ of Jupiter. . . . .	42
4.8	Earth's initial orbit and final orbit are drawn in the $(q_1, q_2)$ plane as the star passes for initial position $(0.195206, 0)$ of Earth. . . . .	45
4.9	Earth's initial orbit's and final orbit's eccentricity, semi-major axis, and argument of the perihelion values as the star passes for initial position $(0.195206, 0)$ of Earth. . . . .	45
4.10	Earth's initial orbit and final orbit are drawn in the $(q_1, q_2)$ plane as the star passes for initial position $(0.180591, -0.073465)$ of Earth. . . . .	47
4.11	Earth's initial orbit's and final orbit's eccentricity, semi-major axis, and argument of the perihelion values as the star passes for initial position $(0.138971, -0.1357460)$ of Earth. . . . .	47
4.12	Earth's initial orbit and final orbit are drawn in the $(q_1, q_2)$ plane as the star passes for initial position $(0.195206, 0)$ of Earth. . . . .	48
4.13	Earth's initial orbit's and final orbit's eccentricity, semi-major axis, and argument of the perihelion values as the star passes for initial position $(-0.0702688, -0.17736)$ of Earth. . . . .	48
4.14	Change in global mean temperature for Earth for a few values of eccentricity. . . . .	51
4.15	Change in global mean temperature for Earth for a few values of the semi-major axis. . . . .	52
4.16	Equilibrium temperature profile for Earth for the current and perturbed parameters. . . . .	53
4.17	Bifurcation diagram of the semi-major axis $a_E$ . All other parameters are in table 3.1. . . . .	54

5.1	Jupiter's initial orbit and final orbit are drawn in the $(q_1, q_2)$ plane as the star passes at a distance of 100 AUs. . . . .	60
5.2	Jupiter's initial orbit's and final orbit's eccentricity, semi-major axis, and argument of the perihelion values as the star passes with its closest approach at 100 AUs. . . . .	60
5.3	Jupiter's initial orbit and final orbit are drawn in the $(q_1, q_2)$ plane as the star passes at a distance of 200 AUs. . . . .	61
5.4	Jupiter's initial orbit's and final orbit's eccentricity, semi-major axis, and argument of the perihelion values as the star passes with its closest approach at 200 AUs. . . . .	61
5.5	Change in global mean temperature (GMT) based on the changes found in table 5.2. . . . .	63
5.6	Equilibrium temperature profile for Earth for the current and perturbed parameters when star passes by at 100 AUs away. . . . .	65
5.7	Change in global mean temperature (GMT) based on the changes found in table 5.4. . . . .	68
5.8	Change in global mean temperature (GMT) based on the changes found in table 5.5. . . . .	69
5.9	Equilibrium Temperature Profile based on the changes found in table 5.4 and table 5.5 . . . . .	71

# Chapter 1

## Introduction

The orbits of planets in the Solar System depend upon both the Sun and the positions of the other planets in the system. Disturbances to the orbit of any one of these planets can have an effect on the rest of the Solar System. Gravitational perturbations can be caused by moving objects in space, such as rogue stars. A rogue star is defined as either stars that are free from the constraints of a galaxy (intergalactic rogue stars) or a star that does not follow normal behavior (independent moving stars). A rogue star which came close to the Solar System with high enough mass would be able to change the orbits of the planets and how they interact with each other.

To study if such a star has passed by, scientists and mathematicians look to models of the Solar System. Knowing how the planets move now and their general patterns, the motion of the planets in the past are predicted and how these motions change could indicate the passage of a rogue star. However, the validity of solutions of Solar System gravitational models are constrained to about 0 - 60 million years ago. While relative positions of the major planets remain the same over hundreds of millions of years, details such as the relative phases along orbits can be chaotic, where initially close solutions diverge exponentially [29, 30]. This chaos can make it difficult for scientists to test



physical theories. Although progress on this front has been made in recent years, it is still not possible to retrace the precise history of the Solar System using only current information. On the other hand, Olsen et. al. found a way to use geological data to constrain the astronomical solutions back in time [44].

Indeed, geological data from the last 60 million years agree with astronomical solutions but beyond that there is little information on the Solar System [31, 45]. Olsen et. al. established a method to find empirical data beyond 60 million years ago that uses a network of highly resolved data from multiple temporally correlative and complementary records they call “the Geological Orrery.” This data comes from cores collected from the bottoms of lakes and rivers which can be dated using uranium-lead dating applied to the mineral zircon. The sediments are between 223 and 199 million years old, in the Mesozoic era. The depths of the water were determined by wet and dry ages and Olson et. al. were able to conclude that the orbital changes were responsible for the patterns found in the sediments.

The orbital planes of planets are affected by the gravitational forces of the other bodies in the Solar System in a quasiperiodic manner which can be broken up into a series of secular fundamental frequencies that represent each planet’s contribution to the changes of the orbits. These motions can be described in terms of the precession of the periapsis,  $g_i$  frequencies, in the orbital plane and the precession of the orbital plane itself in space (represented by the precession of the ascending node),  $s_i$  frequencies.

Differences in the  $g_i$  values yields the eccentricity cycles of 100,000 and 405,000 years on Earth while the sums of the  $g_i$  frequencies along with Earth’s axial precession constant,  $p$ , yields the climate precession cycle of about 23,000 years. The sum of the  $s_i$  frequencies along with  $p$  yields the obliquity periodicity of about 41,000 years. These three cycles, obliquity, eccentricity, and precession, are the Milankovitch cycles which inform the oscillatory nature of Earth’s climate. Olsen et. al. reported a 405,000 year

cycle in the sediments, known as the McLaughlin cycle, which matches the eccentricity cycle [44]. Unlike the McLaughlin cycle, most of the other cycles were of different lengths in the Triassic period compared to today. The McLaughlin cycle acts as a measuring stick, for example indicating the length of the precession cycle [44]. The relative phases of these cycles can be ascribed to positions of the inner planets and Jupiter [44].

This allows for mathematicians and scientists to create conditions in the past that the solutions of the orbits of the Solar System must satisfy. As the solutions diverge exponentially, some of the orbits can be ruled out if they do not satisfy the conditions set forth from this coring data [44].

If a star passed within our Solar System at a range that were to affect the Earth's orbit, this would appear in the work done in [44]. The changes spotted in the coring data would then be related back to the secular fundamental frequencies and would indicate the planetary orbits going back several million years. In this paper, the types of changes that would be observed in the orbits of the planets that would occur from a passing star are studied. As changes to elements of the orbit of a planet have effects on the climate of that planet, possible climatic effects are also considered in this work.

Broadly, the point of this work is to study the changes that can be observed by gravitational disturbances to orbits in the Solar System. The focus is placed upon how the eccentricity, semi-major axis, and argument of the periapsis change as a rogue star passes at varying distances.

The first part of this work sets up the equations used to model the Sun-planet-star system that will be focused upon. This modeling is done using a special case of the gravitational  $n$ -body problem and is done throughout the paper in two-dimensions. Then the framework for the climate modeling is also given, with the Budyko-Widiasih equation explained along with its relationship to orbit of planets [6, 35, 56].

In chapter 4, the effects of the rogue star passing the Kuiper Belt are studied. The

effects of this event are calculated both on the orbit of Earth and Jupiter. Jupiter is considered as it is the most massive of the planets in the Solar System and its orbit sets the ecliptic. Changes to Jupiter's orbit could change the secular fundamental frequencies and have effects on Earth's orbit. Additionally, Earth's orbital changes are also considered along with the climatic change that would result from these changes. Here it is shown that such a close star passage almost certainly did not occur as the changes to the eccentricity cycle on Earth would be dramatic and noticeable. As such an occurrence has not been spotted already, it's safe to conclude an encounter this close did not happen.

In chapter 5, the sensitivity of the equations to the distance of the rogue star's passage is analyzed. The star's orbit is moved further and further away from the Solar System to understand where it is that subtle changes can still be observed. As the star moves further away, its effects on the Sun-planet system are diminishing, as expected. The star's effects become so subtle on the orbit of the planet that the changes become negligible. Indeed, the effects still exist but are so small that one could attribute the variation observed to numerical error.

## Chapter 2

# The Hyperbolic Restricted Three-Body Problem

An orbit is the gravitationally curved trajectory of an object, such as the trajectory of a planet around a star or a natural satellite around a planet. Normally, orbit refers to a regularly repeating trajectory, although it may also refer to a non-repeating trajectory. To a close approximation, planets and satellites follow elliptic orbits, with the center of mass being orbited at a focal point of the ellipse, as described by Kepler's laws of planetary motion [25]. For most situations, orbital motion is well approximated by Newtonian mechanics, where gravity is as a force obeying an inverse-square law [26].

Before a star comes by to disturb the solar system, the planets are orbiting the Sun. Focusing on the Sun and the Earth, there are two bodies' motions to consider (see figure 2.1). Note that this planet does not necessarily need to be Earth, but can be any planet that orbits the Sun. In fact, in this paper, both Jupiter's and Earth's orbit around the Sun will be studied.

The Kepler problem is the case in which two bodies interact by a central force that varies in strength as the inverse square of the distance  $r$  between them. The problem is

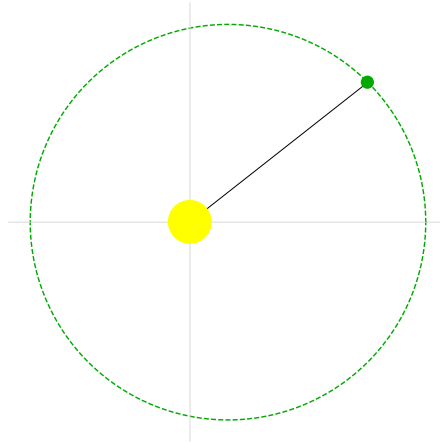


Figure 2.1: Initial two-body problem that is present before the rogue star passes through the system. Here the Earth (green) is orbiting the Sun (yellow) on an orbit of eccentricity 0.0167 [60].

to find the position or speed of the two bodies over time given their masses, positions, and velocities. Kepler motion is governed by the differential equation

$$\ddot{\mathbf{x}}(t) = -\frac{\mu\mathbf{x}(t)}{|\mathbf{x}(t)|^3} \quad (2.1)$$

where  $\mathbf{x} \in \mathbb{R}^n$  denotes the position of the particle, the dot is the derivative with respect to time  $t$ , and  $\mu$  is the gravitational parameter. Using classical mechanics, the solution can be expressed as a Kepler orbit, the motion of one body relative to another as a circle, ellipse, parabola, or hyperbola, which forms a two-dimensional orbital plane in three-dimensional space. Kepler orbits can be parametrized using six orbital elements – eccentricity ( $e$ ), semi-major axis ( $a$ ), inclination ( $i$ ), longitude of the ascending node ( $\Omega$ ), argument of the periapsis ( $\omega$ ), and the true anomaly ( $\nu$ ).

The Kepler problem has a known solution, which is given in polar coordinates ( $r$ ,

$\nu$ ) to be

$$r = \frac{|\mathbf{\Omega}|^2/\mu}{1 + e \cos(\nu)} \quad (2.2)$$

where  $\mathbf{\Omega}$  represents the angular momentum [46]. Based on the value of  $e$ , the solution is either a circle, ellipse, parabola, or hyperbola.

As the star approaches the system, three bodies are taken into consideration – the Sun, the planet that orbits the Sun (e.g. Earth), and the passing star. Let the position of mass  $m_i$  be given by  $\mathbf{x}_i \in \mathbb{R}^n$ . The equations that define the motion of the three bodies are given below.

$$\begin{aligned} \ddot{\mathbf{x}}_1 &= -Gm_2 \frac{\mathbf{x}_1 - \mathbf{x}_2}{|\mathbf{x}_1 - \mathbf{x}_2|^3} - Gm_3 \frac{\mathbf{x}_1 - \mathbf{x}_3}{|\mathbf{x}_1 - \mathbf{x}_3|^3} \\ \ddot{\mathbf{x}}_2 &= -Gm_1 \frac{\mathbf{x}_2 - \mathbf{x}_1}{|\mathbf{x}_2 - \mathbf{x}_1|^3} - Gm_3 \frac{\mathbf{x}_2 - \mathbf{x}_3}{|\mathbf{x}_2 - \mathbf{x}_3|^3} \\ \ddot{\mathbf{x}}_3 &= -Gm_1 \frac{\mathbf{x}_3 - \mathbf{x}_1}{|\mathbf{x}_3 - \mathbf{x}_1|^3} - Gm_2 \frac{\mathbf{x}_3 - \mathbf{x}_2}{|\mathbf{x}_3 - \mathbf{x}_2|^3}, \end{aligned} \quad (2.3)$$

The three-body problem does have a global analytical solution in the form of a convergent power series, but does not have a general analytic solution by algebraic expressions and integrals. This power series solution as was proven by Sundman [52]. However, the Sundman series converges slowly; therefore, it is currently necessary to approximate solutions by numerical analysis.

In order to study the motion of the elliptic orbit of the planet when it is perturbed by a passing star, one can reduce the problem from the complexities of a general three body problem (equation (2.3)) with the use of the following assumptions:

1. Two finite masses,  $m_1$  and  $m_2$ , have hyperbolic orbits with respect to their center of mass, and hence, each has a hyperbolic orbit with respect to the other. These are referred to as the primary masses.

2. A third body of infinitesimal mass is in the system which does not affect the motion or location of the center of mass of the two primary masses. In the case studied here, the Earth's mass is 333,000 smaller than that of the Sun and Jupiter's mass is 1,047 smaller than the Sun [58, 59], allowing for such an assumption to make sense.

The first assumption defines the Hyperbolic Three-Body Problem. The second assumption defines the Restricted Three-Body Problem, where the mass of a much smaller object is approximated to be zero. This allows the other two bodies in the system (the primaries) to create a two-body problem, which is solvable. The third body then moves in the vector field created by the interaction of the primaries. Together, this gives us the Hyperbolic Restricted Three-Body Problem (HR3BP).

In this chapter, the HR3BP is set-up in a relative coordinate system that to mirror the Sun-planet-star system considered in this paper more closely. Then, regularization methods are applied to create more stability in the numerical integration of the system. Lastly, other literature on the HR3BP is presented and the approaches are compared to the one used in this paper.

## 2.1 Conserved Quantities, Symmetries, and Integrals of Motion

A Hamiltonian system is a dynamical system that is completely described by a scalar function  $\mathcal{H}(\mathbf{x}, \mathbf{y}, t)$ , known as the Hamiltonian, where  $\mathbf{x}, \mathbf{y} \in \mathbb{R}^2$ . The differential equations for the system are given by the Hamiltonian as follows:

$$\dot{\mathbf{x}} = \frac{\partial \mathcal{H}}{\partial \mathbf{y}}(\mathbf{x}, \mathbf{y}), \quad \dot{\mathbf{y}} = -\frac{\partial \mathcal{H}}{\partial \mathbf{x}}(\mathbf{x}, \mathbf{y}). \quad (2.4)$$

Here,  $(\mathbf{x}(t), \mathbf{y}(t))$  is the solution of the IVP defined by equation (2.4), known as Hamilton's equations, and an initial condition  $(\mathbf{x}(t_0), \mathbf{y}(t_0)) = (\mathbf{x}_0, \mathbf{y}_0)$ . For equation (2.3), the Hamiltonian is given to be

$$\mathcal{H} = -\frac{Gm_1m_2}{|\mathbf{x}_1 - \mathbf{x}_2|} - \frac{Gm_2m_3}{|\mathbf{x}_3 - \mathbf{x}_2|} - \frac{Gm_3m_1}{|\mathbf{x}_3 - \mathbf{x}_1|} + \frac{\mathbf{y}_1^2}{2m_1} + \frac{\mathbf{y}_2^2}{2m_2} + \frac{\mathbf{y}_3^2}{2m_3}, \quad (2.5)$$

where  $\dot{\mathbf{x}} = \mathbf{y}$  and the second order equation (2.3) is converted to a system of first order equations. Here,  $\mathcal{H}$  does not depend explicitly on time, and as such the Hamiltonian is a constant of motion, equaling the total energy of the system (gravitational plus kinetic).

Symmetries in the three-body problem yield global integrals of motion that simplify the problem [39]. Translation symmetry of the problem results in the center of mass

$$\mathbf{C} = \frac{m_1\mathbf{x}_1 + m_2\mathbf{x}_2 + m_3\mathbf{x}_3}{m_1 + m_2 + m_3}$$

moving with constant velocity, so that  $\mathbf{C} = \mathbf{L}_0t + \mathbf{C}_0$ , where  $\mathbf{L}_0$  is the linear velocity and  $\mathbf{C}_0$  is the initial position. The constants  $\mathbf{L}_0$  and  $\mathbf{C}_0$  represent four integrals of motion.

Rotational symmetry results in the total angular momentum being constant

$$\mathbf{\Omega} = \mathbf{x}_1 \times \mathbf{y}_1 + \mathbf{x}_2 \times \mathbf{y}_2 + \mathbf{x}_3 \times \mathbf{y}_3,$$

where  $\times$  is the two-dimensional cross product. The two components of the total angular momentum  $\mathbf{\Omega}$  yield two more constants of the motion.

The integrals  $\mathbf{C}_0$ ,  $\mathbf{L}_0$ , and  $\mathbf{\Omega}$  provide six constants of motion, and the Hamiltonian,  $\mathcal{H}$ , is the seventh.



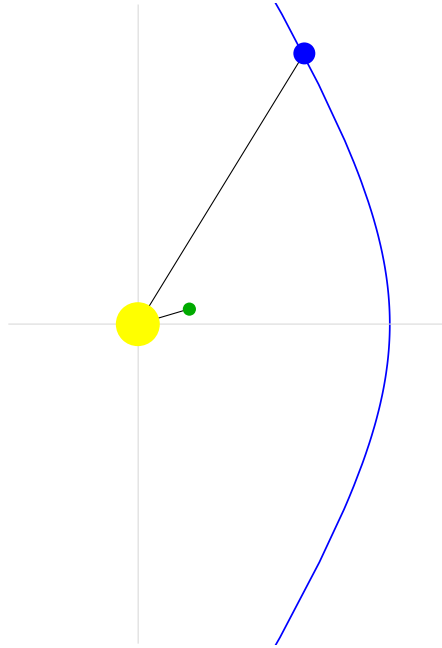


Figure 2.2: Coordinate system created relative to the Sun (whose mass is given by  $m_1$ ). The Sun is located at the focus of the orbit of the planet. The location of the Sun is designated as the origin of the coordinate system.

## 2.2 Relative Coordinate System

The problem considered in this paper is done in the plane, that is,  $\mathbf{x}_1, \mathbf{x}_2, \mathbf{x}_3 \in \mathbb{R}^2$ . In this system, let  $m_1$  represent the Sun,  $m_2$  represent the passing star, and  $m_3$  represents the planet. We are interested in solutions where the planet stays close to the Sun, and as such we look at a coordinate system relative to the Sun (see figure 2.2).

Let

$$\mathbf{Q} = \mathbf{x}_2 - \mathbf{x}_1 \quad \text{and} \quad \mathbf{q} = \mathbf{x}_3 - \mathbf{x}_1,$$

where  $\mathbf{Q}, \mathbf{q} \in \mathbb{R}^2$ . Taking into account that  $m_3 = 0$ , and choosing the units of mass

properly so  $G = 1$ , the equations of motion can be derived from equation (2.3).

$$\ddot{\mathbf{Q}} = -\frac{(m_1 + m_2)\mathbf{Q}}{|\mathbf{Q}|^3} \quad (2.6)$$

$$\ddot{\mathbf{q}} = -\frac{m_1\mathbf{q}}{|\mathbf{q}|^3} - \frac{m_2(\mathbf{q} - \mathbf{Q})}{|\mathbf{q} - \mathbf{Q}|^3} - \frac{m_2\mathbf{Q}}{|\mathbf{Q}|^3} \quad (2.7)$$

Equation (2.6) is the Kepler problem (see equation (2.1)), and as such, there is a closed form solution in the form of polar coordinates (see Equation equation (2.2)). This equation describes the relative motion of the two stars, which is set to be a hyperbola. Such a solution can be characterized by two parameters  $a > 0$  and  $e > 1$ . There is no simple formula for the solution  $\mathbf{Q}(t)$ , but defining both  $Q$  and  $t$  in terms of the hyperbolic anomaly,  $E$ , the solution can be parametrized by the following equations [22].

$$\mathbf{Q}(t) = R \begin{pmatrix} \cos(\nu) \\ \sin(\nu) \end{pmatrix} \quad (2.8)$$

$$R(E) = a(e \cosh(E) - 1) \quad (2.9)$$

$$\tan\left(\frac{\nu}{2}\right) = \sqrt{\frac{e+1}{e-1}} \tanh\left(\frac{E}{2}\right) \quad (2.10)$$

$$e \sinh(E) - E = \sqrt{\frac{m_1 + m_2}{a^3}} t \quad (2.11)$$

Equation (2.10) can be rewritten with the substitution

$$\tau = \tan\left(\frac{\nu}{2}\right),$$

then

$$\cos(\nu) = \frac{1 - \tau^2}{1 + \tau^2} \quad \text{and} \quad \sin(\nu) = \frac{2\tau}{1 + \tau^2}.$$

Thus, equation (2.8) can be written as a function parametrized by the hyperbolic

anomaly,  $E$ , and is the solution of equation (2.6).

This solution can then be used to solve equation (2.7) to determine the motion of Earth's orbit as the rogue star passes through the system. Note that equation (2.7) is very similar to the Kepler problem, equation (2.1), but with an added term  $\mathbf{F}(\mathbf{q}, t)$  where

$$\mathbf{F}(\mathbf{q}, t) = -\frac{m_2(\mathbf{q} - \mathbf{Q})}{|\mathbf{q} - \mathbf{Q}|^3} - \frac{m_2\mathbf{Q}}{|\mathbf{Q}|^3}.$$

### 2.2.1 Regularization Methods

Regularization is a transformation of both space and time variables, introduced by Levi-Civita in the plane and generalized by Kustaanheimo and Stiefel in space [28, 33]. Historically, regularization was developed for investigating singularities of Kepler motion and for describing collisions of two point masses as well as for improving the numerical integration of collision and near-collision orbits.

The Sun and the rogue star are modeled in a manner that ensures that they will not collide or get very close to each other. However, Earth's orbit is modeled to be close to the Sun's, requiring regularization methods to aid the accuracy of numerical solutions. Equation (2.7) models the Earth's motion, relative to the Sun. Let  $\dot{\mathbf{q}} = \mathbf{p}$ , where  $\mathbf{p}$  is the momentum. Then equation (2.7) can be converted to a system of first order ODEs.

$$\dot{\mathbf{q}} = \mathbf{p} \tag{2.12}$$

$$\dot{\mathbf{p}} = -\frac{m_1\mathbf{q}}{|\mathbf{q}|^3} - \frac{m_2(\mathbf{q} - \mathbf{Q})}{|\mathbf{q} - \mathbf{Q}|^3} - \frac{m_2\mathbf{Q}}{|\mathbf{Q}|^3} \tag{2.13}$$

The time-dependent Hamiltonian of the system created by equation (2.12) and equation (2.13) is

$$\mathcal{H}(\mathbf{q}, \mathbf{p}, t) = \frac{1}{2}|\mathbf{p}|^2 - \frac{m_1}{|\mathbf{q}|} - \frac{m_2}{|\mathbf{q} - \mathbf{Q}|} - \frac{m_2}{|\mathbf{Q}|}. \tag{2.14}$$

Let the Kepler energy of  $(\mathbf{q}, \mathbf{p})$  be given by

$$\mathcal{K}(\mathbf{q}, \mathbf{p}) = \frac{1}{2}|\mathbf{p}|^2 - \frac{m_1}{|\mathbf{q}|} = -h < 0$$

where  $h > 0$  is a real constant. The value of  $\mathcal{K}(q, p)$  is necessarily negative since the planets orbit the Sun in an ellipse before the rogue star passes.

### Levi-Civita Regularization

The Levi-Civita regularization introduces a new time variable and creates a conformal squaring map. Complex notation will be used throughout, i.e. instead of the vector  $\mathbf{x} = \begin{pmatrix} x_1 \\ x_2 \end{pmatrix} \in \mathbb{R}^2$ , the corresponding complex coordinate  $x = x_1 + ix_2 \in \mathbb{C}$  will be used.

The Levi-Civita transformation [33, 51] is given by the equations

$$q = 2z^2 \tag{2.15}$$

$$p = \frac{w}{\bar{z}}. \tag{2.16}$$

Additionally, in the place of the physical time  $t$ , a new independent time variable  $\tau$  is introduced by the differential equation

$$dt = 2|z|^2 d\tau. \tag{2.17}$$

Let derivatives with respect to  $\tau$  be denoted by primes. Then the system of equation (2.12) and equation (2.13) becomes

$$z'(\tau) = \frac{1}{2}w \tag{2.18}$$

$$w'(\tau) = -hz - 2|z|^2 z \cdot F(2z^2, t(\tau)) \tag{2.19}$$

with the Kepler energy of  $(z, w)$  given by

$$\frac{|w|^2}{2|z|^2} - \frac{m_1}{2|z|^2} = -h. \quad (2.20)$$

Note that this is not the Hamiltonian for the non-perturbed problem defined by

$$\begin{aligned} z'(\tau) &= \frac{1}{2}w \\ w'(\tau) &= -hz, \end{aligned}$$

Instead, we find the value for the new energy surface by looking at the isoenergetic reduction and find that the Hamiltonian for the system is actually given by [63]

$$\tilde{\mathcal{K}}(z, w) = \frac{1}{2}|w|^2 + h|z|^2 = \frac{m_1}{4}. \quad (2.21)$$

The system of equations defined by equation (2.18) and equation (2.19) are regularized in the sense that the singularity at the origin has been eliminated from the original system of equation (2.12) and equation (2.13).

Translating equation (2.14) to Levi-Civita coordinates yields the equation

$$\frac{|w|^2}{2|z|^2} - \frac{m_1}{2|z|^2} - \frac{m_2}{|q - Q(t)|} - \frac{m_2}{|Q(t)|}.$$

The Hamiltonian for the system of equations equations (2.18) and (2.19) is given to be

$$\tilde{\mathcal{H}}(z, w, \tau) = \frac{1}{2}|w|^2 + h|z|^2 - \frac{m_2|z|^2}{|2z^2 - Q(t(\tau))|} - \frac{m_2}{|Q(t(\tau))|} \quad (2.22)$$

In both the system of equations given by equations (2.18) and (2.19) and equation (2.22),  $t$  is written as a function of  $\tau$ . Given that the relationship between the two that is known is given by equation (2.17), it will get added to the set of ODEs that will get solved.

Lastly, recall that  $h$  is no longer a constant, but a function of time as well. Putting all this together yields the following system of equations

$$\begin{aligned}
 z' &= \frac{w}{2} \\
 w' &= -hz - 2|z|^2 z F(2z^2, t) \\
 h' &= 2F(2z^2, t) \cdot zw \\
 t' &= 2|z|^2
 \end{aligned} \tag{2.23}$$

Since  $h, t \in \mathbb{R}$ , this is a six dimensional system.

Recall that equation (2.8) was parametrized by the hyperbolic anomaly,  $E$ . As  $Q$  can be thought of as  $Q(E)$ , The function  $F(q, t)$  can instead be thought of as  $F(q, E)$ , which becomes easier to evaluate given how  $Q$  is parametrized by  $E$ . The ODE for  $E'$  can be substituted in the place of  $t'$ .

$$\begin{aligned}
 z' &= \frac{w}{2} \\
 w' &= -hz - 2|z|^2 z F(2z^2, E) \\
 h' &= 2F(2z^2, E) \cdot zw \\
 E' &= \frac{2|z|^2}{e \cosh(E) - 1}
 \end{aligned} \tag{2.24}$$

Equations (2.24) defines the motion of the planet in the vector field created by the interactions of the Sun and the passing star in the planar situation.

### 2.3 Other Work on the HR3BP

The problem of finding the general solution of the  $n$ -body problem was considered very important and challenging and can find its roots in the time of Ptolemy. Indeed, looking at solutions of the HR3BP is not a new problem, and various other approaches exist.

There's a body of work focused on describing the motion of the third body which is in third body moves on a straight line perpendicular to the line of motion of the two primaries [8, 9, 10]. Work has also been done with restricting the motion of all three bodies to the unit circle [34]. Two different studies on the HR3BP are elaborated upon below as these both specifically consider the case where the third body is in an elliptic orbit around one of the primaries [21, 49].

### 2.3.1 Approach by Faintich

Faintich studied the equations of motion for the HR3BP for a Sun-star-comet system where the equations were studied in a set of non-rotating axes centered on the Sun with the hyperbolic anomaly as the independent variable [21]. In this set-up, the Sun and the passing star are in hyperbolic orbits in the plane, and the third body, the comet is allowed to approach from outside the plane and hence the equations of motion are in three dimensions (see equations (2.25) to (2.27)). Here,  $d_1$  represents the distance to the star and  $d_2$  the distance to the Sun.

$$\begin{aligned} \frac{d^2 q_1}{dE^2} - \frac{e \sinh(E)}{(e \cosh(E) - 1)} \frac{dq_1}{dE} - \frac{m_1 a}{(m_1 + m_2)} \left( \cosh(E) - \frac{e \sinh^2(E)}{(e \cosh(E) - 1)} \right) \\ + \frac{a^3 (e \cosh(E) - 1)^2}{(m_1 + m_2)} \left( \frac{m_1 (q_1 + a(e - \cosh(E)))}{d_1^3} + \frac{m_2 q_1}{d_2^3} \right) = 0; \end{aligned} \quad (2.25)$$

$$\begin{aligned} \frac{d^2 q_2}{dE^2} - \frac{e \sinh(E)}{(e \cosh(E) - 1)} \frac{dq_2}{dE} + \frac{m_1 a \sqrt{e^2 - 1}}{(m_1 + m_2)} \left( \sinh(E) - \frac{e \sinh(E) \cosh(E)}{(e \cosh(E) - 1)} \right) \\ + \frac{a^3 (e \cosh(E) - 1)^2}{(m_1 + m_2)} \left( \frac{m_1 (q_2 + a \sqrt{e^2 - 1} \sinh(E))}{d_1^3} + \frac{m_2 q_2}{d_2^3} \right) = 0; \end{aligned} \quad (2.26)$$

$$\frac{d^2 q_3}{dE^2} - \frac{e \sinh(E)}{(e \cosh(E) - 1)} \frac{dq_3}{dE} + \frac{a^3 (e \cosh(E) - 1)^2}{(m_1 + m_2)} \left( \frac{m_1 q_3}{d_1^3} + \frac{m_2 q_3}{d_2^3} \right) = 0. \quad (2.27)$$

Faintich's applies these equations to a hypothetical star-sun-comet system to determine the effect of the stellar encounter on the orbit of the comet. The comet is initially in a near-parabolic orbit around the Sun ( $e = 0.999980$ ) starting around 50,000 AU

away from the Sun. The passing star is considered to affect the Sun-comet system for a finite time period.

Various numerical examples are integrated from  $\nu = -1.5$  to  $\nu = 1.5$  (see table 1 in [21]). Some initial conditions show that the stellar passage changed the path of the comet; if unperturbed, the comet could have come into the Solar System so far as to be detected from Earth. However, the comet's interaction with the passing star changed its trajectory and it would remain undetected.

### 2.3.2 Approach by Sorokovich

Sorokovich analyzed the single-averaged HR3BP in the plane [49]. The first body and second body are placed in hyperbolic orbits with respect to each other, but the coordinate system used places the first body at the origin (similar to the Sun in the system studied in this paper). The third body with very small mass is assumed close to the first body (similar to the Earth in the system studied in this paper). The perturbation function of the problem is given by the equation

$$F = m_2 \left( \frac{1}{\sqrt{q^2(t) + Q^2(t) - 2q(t)Q(t)\cos(\alpha)}} - \frac{q(t)\cos(\alpha)}{Q^2(t)} \right) \quad (2.28)$$

where  $\alpha$  is the angle between  $q(t)$  and  $Q(t)$  and is the sum of the true anomalies of the orbits of the second body ( $\tilde{\nu}$ ) and the third body ( $\nu$ ) and the argument of the periapsis of the third body ( $\omega$ ) [18]. Assuming that  $q(t) \ll Q(t)$ , [49] expands equation (2.28) in a series in powers of  $\frac{q(t)}{Q(t)}$ . Discard from this expansion the term not dependent on the coordinate of the perturbing body, the second body, the expansion is

$$F = \frac{m_2}{Q(t)} \sum_{k=2}^{\infty} \left( \frac{q(t)}{Q(t)} \right)^k P_k(\cos(\alpha)), \quad (2.29)$$



where  $P_k(\cos(\alpha))$  is a Legendre polynomial of  $k^{\text{th}}$  order. Averaging  $F$  over the mean anomaly  $M$  yields

$$\bar{F} = \frac{1}{2\pi} \int_0^{2\pi} F dM = \frac{m_2}{a^2 \sqrt{1-e^2}} \sum_{k=2}^{\infty} \frac{1}{Q^{k+1}(t)} \frac{1}{2\pi} \int_0^{2\pi} q^{k+2}(t) P_k(\cos(\alpha)) d\nu \quad (2.30)$$

where

$$dM = \frac{q^2(t) d\nu}{a^2 \sqrt{1-e^2}}, \quad (2.31)$$

where  $a$  and  $e$  are the semimajor axis and eccentricity of the third body. Assuming that the fourth order terms are negligible due to the fact that  $q(t) \ll Q(t)$ , only the first order term is retained and the equation becomes

$$\bar{R} = \frac{m_2}{a^2 \sqrt{1-e^2} Q^3(t)} \frac{1}{2\pi} \int_0^{2\pi} q^4(t) P_2(\cos(\alpha)) d\nu. \quad (2.32)$$

Using a series expansion on  $q(t)$ , assuming it is in the form of an ellipse, and  $Q(t)$ , assuming it forms a hyperbola, the value for  $P_2(x)$ , and changing to  $\tilde{\nu}$  as the independent variable instead of  $t$ , ODEs can be derived to study the motion of the third body [1, 49].

$$\frac{de}{d\tilde{\nu}} = \frac{15}{4} \beta e \sqrt{1-e^2} (1 + \tilde{e} \cos(\tilde{\nu})) \sin(2(\omega - \tilde{\nu})) \quad (2.33)$$

$$\frac{d\omega}{d\tilde{\nu}} = \frac{3}{4} \beta \sqrt{1-e^2} (1 + \tilde{e} \cos(\tilde{\nu})) (1 + 5 \cos(2(\omega - \tilde{\nu}))) \quad (2.34)$$

where

$$\beta = \left( \frac{m_2}{m_1} \right)^{1/2} \left( \frac{a}{\tilde{\ell}} \right)^{3/2}$$

with  $\tilde{\ell}$  the semi-latus rectum and  $\tilde{e}$  is eccentricity of of the orbit of the second body.

Sorokovich's results suggest that the stability of the unperturbed motion holds when

the orbital eccentricity of the third body is small and it remains close to the first body. The exact and singly averaged equations (equation (2.33)) were integrated numerically and it was found that while the eccentricity of the orbit of the third body changes as the second body passes close by, it returns back to its original state eventually. More interestingly, the argument of the periapsis changes by a small amount as the second body passes and it does not return to its original state.

## 2.4 Discussion

In this chapter, the equations of motion for the Sun-planet-star system that is to be studied were derived, see equation (2.6) and equation (2.7). These equations describe the relative motion with respect to a non-rotating coordinate system where the Sun is set at the origin in the plane, and at the focus of the orbit of the planet. Furthermore, regularization techniques were applied to improve numerical integration techniques going forward (discussed in chapters 4 and 5), see equation (2.24).

Two other studies of the HR3BP were also considered in this chapter. In Faintich's work, the third body is in a nearly parabolic orbit. This eccentricity is much higher than the eccentricities of orbits considered in this paper. In fact, the largest eccentricities of the orbit of planets in the Solar System are just a little above 0.2 [61]. Faintich also allows the comet to move in three dimensions, whereas the third body in the equations of this paper are restricted to movement in the plane (see equations (2.12) and (2.13)) and their equations are not in Hamiltonian form. In Sorokovich's work, the set-up is similar to the Sun-planet-star system of this paper but the perturbing effect of the equivalent of the passing star is averaged over the mean anomaly of the orbit. Averaging over the orbit allows for more analytical results to be proven about how the motion could change, but the exact numerical values where events occur along the orbit are lost. As this paper is focused on these numerical values, averaging is not done.

## Chapter 3

# Energy Balance Models

Energy balance climate models, often referred to as energy balance models (EBMs), gained popularity in the late 1960s with the publications of papers by Mikhail Budyko and William Sellers [6, 47]. EBMs are low-dimensional models that attempt to model Earth's surface temperature distribution by the constraint of energy conservation with a few parameters such as the solar radiation and planetary albedo (reflectivity) [6, 47, 55, 56]. As high-speed computers have become more easily accessible, larger scale General Circulation Models (GCMs) have become more prominent in the study of Earth's climate. While GCMs try to take into consideration the incredible complexity of the real climate system, an incredible amount of data is required to constrain all the phenomenological coefficients and it is not always clear how sensitive the results are to the parameters or variables [43].

EBMs continue to be vital tools in the understanding of Earth's climate. These models describe global behaviors of the climate system, whereas GCMs give more local results. For example, EBMs give results about general trends of sea-ice from the phenomenon of ice-albedo feedback, but will not give results on what locations in the arctic will have sea-ice [56]. The low-dimensional characteristic of EBMs make them easy to

modify and run to equilibrium, making them good choices for the study of paleoclimatology. Early research using EBMs was concerned with finding the causes of ice ages and to investigate climate forcings over the past few hundred years [11, 13, 14, 15, 42, 48]. EBMs have also been useful in modeling the distant past [12, 16, 41].

In this chapter, the Budyko-Widiasih EBM is described along with its assumptions. The effects of two specific orbital elements, the semi-major axis and the eccentricity, on the equilibrium temperature profile generated from this EBM are discussed.

### 3.1 Description of the Model

The energy balance equation describes the evolution of the annual average temperature  $T(y, t)$ , where  $t$  denotes the time in years and  $y$  denotes the sine of the latitude (as explained by North, the latitude  $\theta$  is more easily represented by  $y$  as  $y$  is directly proportional to surface area [40]). Here, symmetry about the equator is assumed and so  $0 \leq \theta \leq \frac{\pi}{2}$  or  $0 \leq y \leq 1$ . Let  $\beta$  represent the obliquity. The temperature evolves based on the equation

$$R \frac{\partial T}{\partial t} = Qs_6(y, \beta) (1 - \alpha(y, \eta)) - (A + BT(y, t)) - C (T(y, t) - \bar{T}(t)) \quad (3.1)$$

where the change in temperature is determined by the absorbed solar radiation given by the term  $Qs_6(y, \beta) (\alpha(y, \eta))$ , the outgoing radiation  $(A + BT(y, t))$ , and the transportation of heat between the latitudes  $C (T(y, t) - \bar{T}(t))$ . This continuous adaptation of Budyko's original difference model was done by Tung [6, 54]. Futher, McGehee and Lehman combined the Budyko model version formulated by Tung with Earth's orbital parameters and compared it with the climate data [35]. In addition to equation (3.1),

Widiasih's dynamic ice-line equation

$$\frac{d\eta}{dt} = \varepsilon (T(\eta, t) - T_c) \quad (3.2)$$

is considered [56]. The movement of the ice line is determined by the temperature at the ice line relative to a critical temperature  $T_c$ , where ice forms

### 3.1.1 Absorbed Solar Radiation

The incoming energy at any point on a planet depends upon the location of the point, the planet's orbital parameters (e.g. obliquity), the position of the planet along its orbit, and the solar energy output. Using Kepler's laws and integrating over an entire year, it can be shown that the global annual average power flux is given by

$$Q(a, e) = \frac{Ka^2}{\sqrt{1 - e^2}} \quad (3.3)$$

where  $K$  is proportional to the solar output,  $a$  is the semi-major axis of the planet's orbit, and  $e$  is the eccentricity [35].  $Q$  represents the amount of energy received from the Sun at the top of the atmosphere.

The function  $s(y)$  is the latitudinal distribution of that energy, which can be computed from the Earth's orbital elements. For planet like Earth where all longitudes see the Sun with equal frequency, the annual average insolation distribution reduces to a function only of obliquity  $\beta$  and latitude  $\theta$

$$s(\theta, \beta) = \frac{2}{\pi^2} \int_0^{2\pi} \sqrt{2 - (\cos(\theta) \sin(\beta) \sin(\gamma) - \sin(\theta) \cos(\beta))^2} d\gamma \quad (3.4)$$

where  $\gamma$  is the longitude [35]. As latitude is measured from the Equator, recall that  $0 \leq \gamma \leq \pi/2$ . Obliquity is the angle between the angular momentum vector of the

planetary orbit and the angular momentum vector of the planetary spin, so  $0 \leq \beta \leq \pi$ . Although equation (3.4) gives the insolation, using the integral formula can be quite cumbersome and time consuming. To bypass the issue, North explicitly gives a second-degree approximation for the insolation distribution for the Earth as

$$s(y) = 1 - 0.482 P_2(y)$$

stating that the approximation to the actual distribution is accurate to within 2% of the integral formulation [40]. Here  $P_2(y)$  represents the second Legendre polynomial. North notes that this approximation was first given by Chylek and Coakley as a linear interpolation of the insolation distribution, although no closed-form formula is given in that paper [7]. It should be noted that this quadratic approximation has been used widely. This approximation was computed only for the current obliquity of Earth, and so it cannot be used to compute changes due to the Milankovitch cycles. Nadeau and McGehee's sixth degree approximation,

$$s_6(y, \beta) = 1 - \frac{5}{8} P_2(\cos(\beta)) P_2(y) - \frac{9}{64} P_4(\cos(\beta)) P_4(y) - \frac{65}{1024} P_6(\cos(\beta)) P_6(y), \quad (3.5)$$

which is dependent upon obliquity  $\beta$ , will be used instead [38].

The fraction of the radiative energy absorbed by the planet at point  $y$ , given that the ice line is at  $\eta$ , is represented by the factor

$$1 - \alpha(y, \eta).$$

For each  $\eta$ ,  $\alpha(y, \eta)$  is a real valued function over the  $y$ -interval. Assume that the surface is either water (ice-free) or ice-covered and that there is only one ice-line  $\eta$ . Note that ice

reflects more sunlight than ocean does, and so the surface covered with ice has higher albedo than that covered with ocean. The albedo function that will be used here is piecewise constant given by

$$\alpha(y, \eta) = \begin{cases} \alpha_{ice}, & y > \eta \\ \frac{\alpha_{ice} + \alpha_{H_2O}}{2} & y = \eta \\ \alpha_{H_2O} & y < \eta \end{cases} \quad (3.6)$$

Recall that a symmetry assumption is being made, meaning that whatever happens in the northern hemisphere also happens in the southern hemisphere. Assume the planet has an ice cap, such as Earth does. That is, the ice is located above the ice line and there is water below the ice line.

### 3.1.2 Outgoing Radiation

The incoming radiative energy described in section 3.1.1 is balanced by the reemission of energy along with the transport term (section 3.1.3). The “energy out” is given by the reemission term

$$-(A + BT(y, t)) \quad (3.7)$$

which takes into account many phenomena, such as the Stefan-Boltzmann law of black body radiation and the greenhouse gas effect on the atmosphere. The parameters  $A$  and  $B$  used were determined empirically from satellite data [54]. Note that Kaper and Engler mention in their book that linearizing the Stefan-Boltzmann law overestimates the values of  $A$  and  $B$  for Earth gotten from this satellite data [24].

### 3.1.3 Transport

The energy is transported from warmer latitudes to cooler latitudes and this phenomenon is approximated by the term

$$C (T(y, t) - \bar{T}(t)) \tag{3.8}$$

where the constant  $C$  is a parameter chosen to fit solutions to the current climate of Earth [54]. This transport term is a simpler linear relaxation to the mean annual global temperature, where

$$\bar{T}(t) = \int_0^1 T(y, t) dy$$

is the mean annual global temperature. Many phenomena are included in this term as well, mostly atmospheric and oceanic circulation. While it may seem a simplified approach, many studies have shown that this approximation reproduces relevant results when applied to Earth ([36, 56], among many others). Alternatively, one can model heat transport using a diffusion term as Sellers did in his original work [47]. In this paper, this possibility is not explored.

### 3.1.4 Dynamic Ice Line

The main idea behind the ice line equation is as follows: if the average temperature across the ice line is above the critical temperature, some ice will melt, moving the ice line toward the pole. If it is below the critical temperature, the ice will advance toward the equator. Equation (3.2),

$$\frac{d\eta}{dt} = \varepsilon (T(\eta, t) - T_c)$$

has two important parameters:  $\varepsilon$  and  $T_c$ .  $T_c$ , the critical temperature, is often cited as  $-10$  °C [54]. There parameter  $\varepsilon$  controls how fast the ice line changes in relation to the



temperature and therefore must be positive. When  $\varepsilon = 0$ , the ice lines do not move when the temperature changes and instead the temperature moves as a result of the location of the ice. This is not physical. In the limit as  $\varepsilon$  approaches infinity, The ice line moves instantaneously to changes in the temperature, but this is also not realistic.

### 3.1.5 Values of Parameters in the Budyko Model

Parameter	Name	Value	Units
$R$	surface layer heat capacity	12.6	$\text{W m}^{-2} \text{K}^{-1}$
$K$	solar output	342.998	$\text{W m}^{-2}$
$a$	semi-major axis	1.00000011	AU
$e$	eccentricity	0.0167	dimensionless
$\beta$	obliquity	23.44	degrees
$\alpha_{ice}$	albedo of the ice	0.62	dimensionless
$\alpha_{H_2O}$	albedo of the water	0.32	dimensionless
$A$	greenhouse gas parameter	202	$\text{W m}^{-2}$
$B$	outgoing radiation	1.9	$\text{W m}^{-2} \text{K}^{-1}$
$C$	heat transport	3.04	$\text{W m}^{-2} \text{K}^{-1}$
$\varepsilon$	ice line response to temperature change	varies	$\text{K}^{-1} \text{yr}^{-1}$
$T_c$	critical temperature	-10	$^{\circ}\text{C}$

Table 3.1: Parameter values used in the standard Budyko-Widiasih EBM for Earth.

The values commonly used for the Budyko-Widiasih EBM parameters for Earth are given in table 3.1, along with their units and a brief description. These values can be found in many locations, such as [35, 54, 56, 60].

## 3.2 Effects of the Semi-Major Axis and Eccentricity on Temperature Distribution

According to Laskar et. al, the semi-major axis of Earth’s orbit is essentially constant [32]. This assumption is prevalent throughout work done using the Budyko model (for example, in [35, 56], among many others). If a big enough star were to pass close enough

to our Solar System, the value of the semi-major axis would be affected. To see the effect this orbital element would have on the climate of the planet, the relationship between  $a$  and  $e$  are studied below in the case of constant global annual average power flux given in equation (3.3). The climate record indicates that the eccentricity oscillates between 0 and 0.06 for Earth's orbit [32]. This oscillation creates sufficient changes in Earth's climate that are easily seen in the geological record. Examined here are what changes in the Earth's semi-major axis would have a corresponding impact.

Assuming that the global annual average power flux is constant in equation (3.3), the relationship between small changes in  $e$  and small changes in  $a$  is considered as to understand how the variations in one affect the other. To understand this, let

$$\frac{K(a + \Delta a)^2}{\sqrt{1 - e^2}} = \frac{K a^2}{\sqrt{1 - (e + \Delta e)^2}} \quad (3.9)$$

where  $\Delta e$  represents a small change in eccentricity and  $\Delta a$  represents a small changes in semi-major axis. Then it can be observed that

$$\Delta e = \sqrt{\frac{\left(\frac{\Delta a}{a} + 1\right)^4 + e^2 - 1}{\left(\frac{\Delta a}{a} + 1\right)^4}} - e, \quad (3.10)$$

Figure 3.1 graphs this relationship using the orbital parameter values for Earth's orbit. It is noticeable that small changes to the semi-major axis correspond to stronger changes to the eccentricity values. On Earth, changing the semi-major axis by approximately 0.00141 would be equivalent to changes in the eccentricity of the orbit by 0.06.

Additionally, eccentricity is one of the three Milankovitch cycles and has a 100,000 and 405,000 year cycle [23]. Changes in the eccentricity of the orbit would lead to a disruption of these cycles, visible in the climate record. Eccentricity is of prime importance to glaciation in that it alters the distance the Sun's short wave radiation

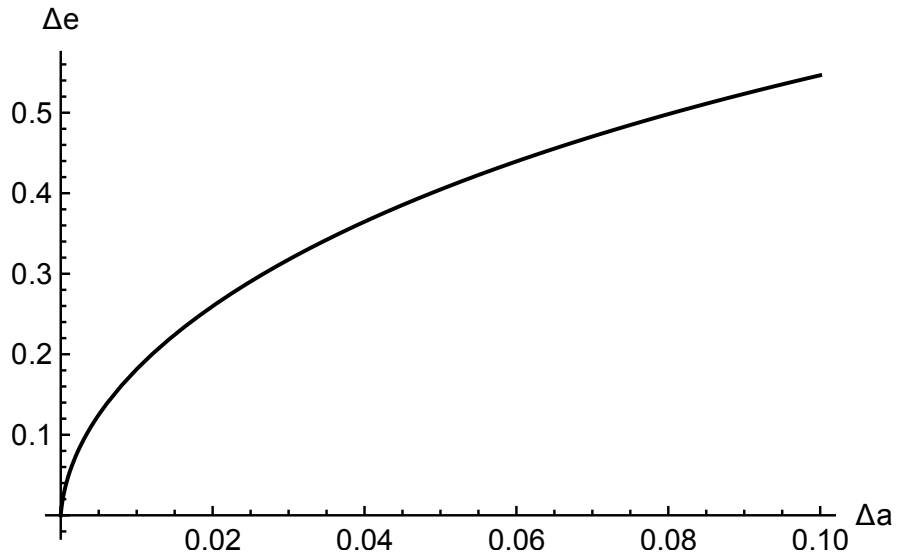


Figure 3.1: Sensitivity of changes in the eccentricity to changes in the semi-major axis.  $e = 0.0167086$  and  $a = 1.00000011$  AU (Earth values).

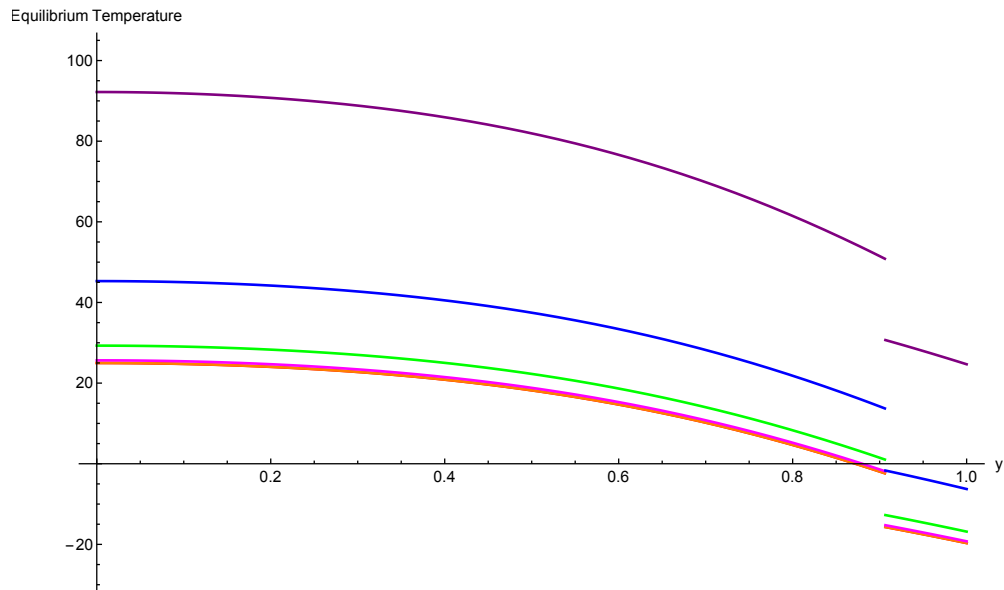


Figure 3.2: Equilibrium temperature profiles using the parameters of Budyko's model for Earth (see table 3.1) for various  $e$  values. Eccentricities drawn are  $e = 0$  (red),  $e = 0.0167$  (orange),  $e = 0.1$  (magenta),  $e = 0.25$  (green),  $e = 0.5$  (blue), and  $e = 0.75$  (purple).  $a$  is held constant at 1 AU. The ice line,  $\eta$  is held constant here at  $66.5^\circ$  N.

must travel to reach Earth, subsequently reducing or increasing the amount of radiation received at the Earth's surface in different seasons.

The equilibrium temperature profile from Budyko's model is given by

$$T^*(\eta, y) = \frac{(Q(a, e) * s_6(y)(1 - \alpha(\eta, y)) - A + C * \bar{T}^*(\eta))}{B + C}. \quad (3.11)$$

A derivation of this equilibrium solution can be found in [56]. The effects on the equilibrium temperature profile due to changes in the eccentricity values can be observed in figure 3.2, where the vertical axis is given in degrees Celsius. In figure 3.2, equation (3.11) is plotted for various values of  $e$  and the values of Earth's orbit were used for all other parameters (see table 3.1). As the eccentricity increases towards 1, the equilibrium temperature profile gets warmer.

### 3.3 Discussion

In this chapter, the Budyko-Widiasih EBM was presented as a way to model a planet's temperature distribution. The model's terms were explained and parameter values were given as well. The sensitivity of changes in the semi-major axis to changes in the eccentricity of the orbit were seen (see figure 3.1). Additionally, the effect that changes in eccentricity would have on the equilibrium temperature profile on Earth were studied.

Assuming the semi-major axis is held constant, equilibrium temperature profiles appeared to increase as orbits became more eccentric. The relative increase in solar irradiation at closest approach to the Sun (perihelion) compared to the irradiation at the furthest distance (aphelion) is slightly larger than four times the eccentricity. Additionally, when Earth's orbit becomes more eccentric, if the semi-major axis is held constant, this necessarily implies that the semi-minor axis shortens. This leads to increases in the magnitude of seasonal changes [3].

## Chapter 4

# Passage in the Kuiper Belt

The gravitational influence of Jupiter has helped shape the solar system. The orbits of most of the system's planets lie closer to Jupiter's orbital plane than the Sun's equatorial plane (Mercury is the only planet that is closer to the Sun's equator in orbital tilt) [59, 61]. In this sense, Jupiter exerts a major influence over the orbital plane of the solar system. In fact, Jupiter contributes over 60% to the invariable, or mean, plane of the solar system (the plane perpendicular to the total angular momentum vector of the solar system that passes through its barycenter) [50]. Earth's orbit is, thus, dependent upon the orbit of Jupiter. If a star were to pass near our Solar System to exert influence upon Earth's climate, it would need to pass close enough to change Jupiter's orbit.

Consider the known stars that have passed or will pass within 5 light-years of the Sun within  $\pm 3$  million years (see table 4.1) [2, 4, 27]. These stars have a higher probability of passing near the Solar System. The average mass of these star is equal to  $0.550556 M_{\odot}$ , or approximately 55% of the mass of the Sun. Thus, this is the value that will be used for the mass of the passing star in the problem set-up.

Star Name	Mass in $M_{\odot}$
Gilse 710	0.4-0.6
Scholz's star and companion brown dwarf	A: 0.095, B: 0.063
HD 283856	$\sim 0.8$
TYC 1662-1962-1	$\sim 0.8$
HD 7977	$\sim 1.2$
2MASS J2146+3813	$\sim 0.15$
2MASS J0634-7449	$\sim 0.6$
TYC 2730-1701-1	$\sim 1$
2MASS J0409+0245	$\sim 0.4$
Gliese 3649	0.49
2MASS J0605+4020	$\sim 0.5$
2MASS J1818-4038	$\sim 0.5$
BD-21 1529	$\sim 0.95$
Ross 248	0.136
Proxima Centauri	0.15
Alpha Centauri AB	A: 1.100, B: 0.907
Gliese 445	0.15?
HIP 117795	$\sim 0.5$
2MASS J0625-2408	$\sim 0.5$
Barnard's Star	0.144
2MASS J2241-2759	$\sim 0.5$
Gliese 3379	0.19
Zeta Leporis	2.0
Lalande 21185	0.39
2MASS J1941-4602	$\sim 0.15$
AVERAGE	0.550556

Table 4.1: Masses of known stars that have passed or will pass within 5 light-years of the Sun within  $\pm 3$  million years measured in  $M_{\odot}$ , where 1  $M_{\odot}$  is the mass of the Sun.

Let the force between the Earth and Jupiter be given by

$$F_d = \frac{Gm_1m_2}{d^2},$$

and the force between the passing star and Earth be given by

$$F_D = \frac{Gm_2M}{D^2},$$

where  $M$  is the mass of the passing star ( $0.550556 M_\odot$ ),  $m_1$  is the mass of Earth ( $3.003 \times 10^{-6} M_\odot$ ),  $m_2$  is the mass of Jupiter ( $9.548 \times 10^{-4} M_\odot$ ),  $G$  is the universal gravitational constant,  $d$  the shortest distance between the Earth and Jupiter (4.206 AU), and  $D$  the shortest distance between the Earth and the passing star. For  $F_d \ll F_D$ ,

$$D^2 \ll \frac{M}{m_1}d^2 \implies D \ll 1800.483244 \text{ AU}.$$

If a star were to pass within approximately 1800 AU from the Sun, it would exert more force on the Earth than Jupiter does. Since Jupiter affects Earth's orbit enough to change its climate, we might expect the event of a star passing this close to the Sun to be observable in the geological record. This distance goes far past the Kuiper Belt, which ranges from approximately 30 AU to 50 AU away from the Sun [17]. The Kuiper Belt is a circumstellar disc region of icy bodies beyond the orbit of Neptune made up of objects composed largely of frozen volatiles (e.g. methane, ammonia, water) [37]. Similar to the asteroid belt, the Kuiper Belt is a region of leftover objects from the solar system's early history.

In this chapter, both the effects on Jupiter, along with Earth, are considered by the passage of a star at the edge of the Kuiper Belt. First the initial conditions are laid out, along with their specific values for simulations. Then, simulation results are given,

along with some discussion of these results. For Earth, the effects on the climate are also considered. The study in this chapter is limited to looking at closer approaches within the Kuiper Belt. Sensitivity to the distance of the star is studied in chapter 5.

## 4.1 Initial Conditions

The initial conditions to consider for this problem involve both the hyperbolic orbit of the passing star and the orbit of Earth and Jupiter around the Sun. The star passes by on a hyperbolic orbit defined by the length of the semi-major axis  $a$  and the eccentricity  $e > 1$ . Equation (2.8) gives this relationship in terms of the hyperbolic anomaly  $E$ . The vertex of the hyperbola is set to be on the  $x$ -axis. This will be at 50 AU from the Sun, the edge of the Kuiper Belt.

The elliptic orbit of the planet, for example Jupiter, can be parametrized with the focus of this orbit, where the Sun is located, at the origin. The following calculations can also be done for Earth's orbit, simply replacing the semi-major axis and eccentricity values with those of the orbit of Earth. The parametrization is

$$q_1(s) = a_J \cos(s) + a_J e_J \tag{4.1}$$

$$q_2(s) = a_J \sqrt{1 - e_J^2} \sin(s) \tag{4.2}$$

$$p_1(s) = -\frac{\sqrt{m_1}}{\sqrt{a_J}(1 + e_J \cos(s))} \sin(s) \tag{4.3}$$

$$p_2(s) = \frac{\sqrt{m_1} \sqrt{1 - e_J^2}}{\sqrt{a_J}(1 + e_J \cos(s))} \cos(s) \tag{4.4}$$

where

$$\frac{ds}{dt} = \frac{m_1^{1/2} a_J^{-3/2}}{1 + e_J \cos(s)}. \tag{4.5}$$



Now the initial conditions are given simply by knowing the eccentricity and semi-major axis of the orbit, which are both known values for Jupiter and Earth [60, 58]. Equation (4.5) comes from the famous Kepler equation and its derivative,

$$t = \sqrt{\frac{a_J^3}{m_1}} (s + e_J \sin(s)),$$

where  $s$  is the eccentric anomaly of the orbit. Recall as well that as Jupiter is on an elliptic orbit, the Hamiltonian will be a constant, negative number. From chapter 2, let

$$\tilde{\mathcal{H}}(\mathbf{q}, \mathbf{p}, t) = \frac{1}{2} |\mathbf{p}|^2 - \frac{m_1}{|\mathbf{q}|} = -h,$$

where  $h = \frac{m_1}{2a}$ .

Equations (4.1) to (4.4) suggest that the eccentric anomaly  $s$  might be a more suitable independent variable. In fact, this relationship is what motivates the Levi-Civita transformation. Using the Levi-Civita transformation given by equations (2.15) and (2.16) to find the initial conditions in the coordinate system used so far yields the parametrization below.

$$z_1(\tau) = \frac{1}{\sqrt{2}} \sqrt{a_J(1+e_J)} \cos\left(\sqrt{\frac{m_1}{a_J}} \frac{\tau}{2}\right) \quad (4.6)$$

$$z_2(\tau) = \frac{1}{\sqrt{2}} \sqrt{a_J(1-e_J)} \sin\left(\sqrt{\frac{m_1}{a_J}} \frac{\tau}{2}\right) \quad (4.7)$$

$$w_1(\tau) = -\frac{1}{\sqrt{2}} \sqrt{\frac{m_1}{a_J}} \sqrt{a_J(1+e_J)} \sin\left(\sqrt{\frac{m_1}{a_J}} \frac{\tau}{2}\right) \quad (4.8)$$

$$w_2(\tau) = \frac{1}{\sqrt{2}} \sqrt{\frac{m_1}{a_J}} \sqrt{a_J(1-e_J)} \cos\left(\sqrt{\frac{m_1}{a_J}} \frac{\tau}{2}\right), \quad (4.9)$$

where

$$s = \frac{1}{2} \sqrt{\frac{m_1}{a_J}} \tau.$$

The Hamiltonian for the Levi-Civita coordinates equation (2.21) from the unperturbed problem gives an extra equation that the initial conditions must satisfy. Namely,

$$h = \frac{m_1 - |w|^2}{2|z|^2}$$

as the orbit starts on the energy surface that this equation satisfies. The semi-major axis and eccentricity of Jupiter's orbit are known values and thus the orbit of Jupiter can be used as the initial condition [58]. An image of the set-up is given in figure 4.1.

Recall again that equations (4.6) to (4.9) are the same initial conditions used for the problem where Earth is the third body, but replacing  $a_J$  with  $a_E$  and  $e_J$  with  $e_E$ .

#### 4.1.1 Values of Parameters in Simulations

The specific values used for the initial conditions in the simulation appear in table 4.2. In the table, a brief description of the parameters, along with their values, are given. The table includes both initial condition values for Jupiter as the third body and Earth as the third body. All initial conditions associated to Jupiter are noted with a  $J$  subscript, similarly all initial conditions associated to Earth are noted with an  $E$  subscript.

## 4.2 Effects on the Orbit of Jupiter

First, Jupiter is considered as the third body and the effects on its orbit are studied. Equation (2.24) were numerically solved using Mathematica, specifically the `NDSolve` function, utilizing the initial conditions described in section 4.1. All initial conditions were set at time `-smax= 500`. This choice was made so that the orbital parameter values settled towards a constant (with little numerical error). The ODE was solved over the time period `[-smax, smax]`.

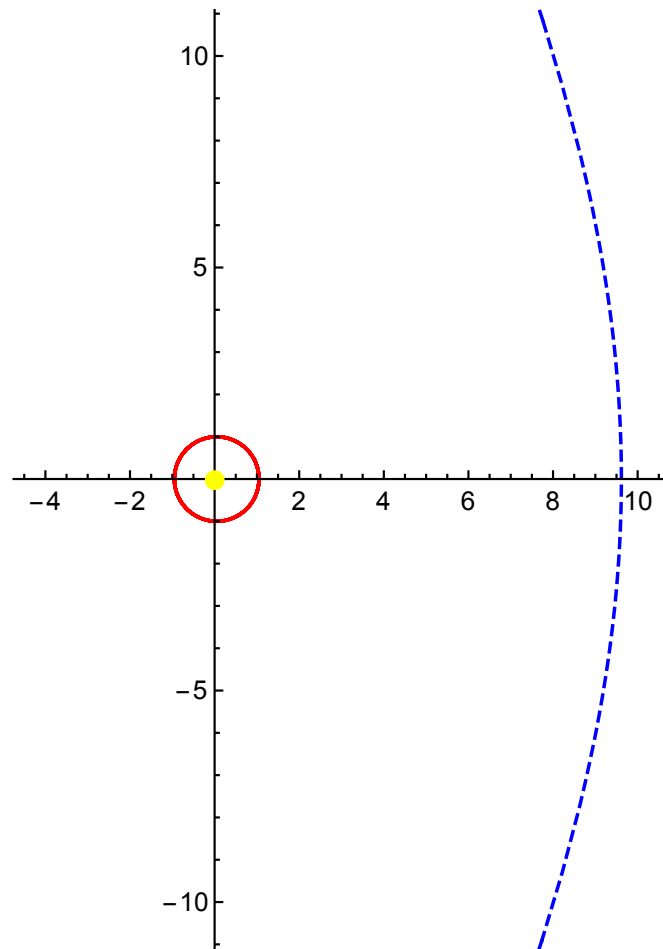


Figure 4.1: The initial set-up of the problem in this chapter is drawn with Jupiter as the third body. The path in red is Jupiter's initial orbit. The dashed blue line details the path the star will travel as time evolves.

Parameter	Name	Value
$a$	semi-major axis of orbit of passing star	9.6153846154
$e$	eccentricity of orbit of passing star	2
$E$	hyperbolic anomaly of orbit of passing star	-3
$a_J$	semi-major axis of orbit of Jupiter	1
$e_J$	eccentricity of orbit of Jupiter	0.0489
$T_J$	period of Jupiter's orbit	7.82391
$\omega_J$	argument of the periapsis of Jupiter's orbit	0
$a_E$	semi-major axis of orbit of Earth	0.192
$e_E$	eccentricity of orbit of Earth	0.0167
$T_E$	period of Earth's orbit	0.658227
$\omega_E$	argument of the periapsis of Earth's orbit	0
$m_1$	mass of Sun	0.6449299
$m_2$	mass of passing star	0.3550701

Table 4.2: Initial conditions of the HR3BP for both Jupiter and Earth as the third body in an elliptic orbit and the star passing in the middle of the Kuiper Belt. The system has been scaled so that Jupiter could be a distance of 1 unit away.

In the simulation, the star take approximately a quarter of an orbit to pass, approximately “three months” time. As the star passes by the solar system, there is a small but noticeable change in Jupiter’s orbit (see figure 4.2). Here, the dashed, grey curve indicates the original orbit while the solid, red curve indicates the final orbit. Additionally, the plot drawn is in the position plane, that is, it is drawn in the  $(q_1, q_2)$ -plane and not the  $(z_1, z_2)$ -plane. The initial orbit is shifted slightly inward, as if the star had pushed orbit away.

As the orbit shifts, so do the orbital elements. Specifically, the eccentricity and semi-major axis of the orbits shift slightly. The final value for the eccentricity of the orbit is an increase of approximately 0.01 (see figure 4.3a). Additionally, the final value for the semi-major axis is a decrease of approximately 3.1% (see figure 4.3b).

The change in the semi-major axis results in a change to the orbital period of the

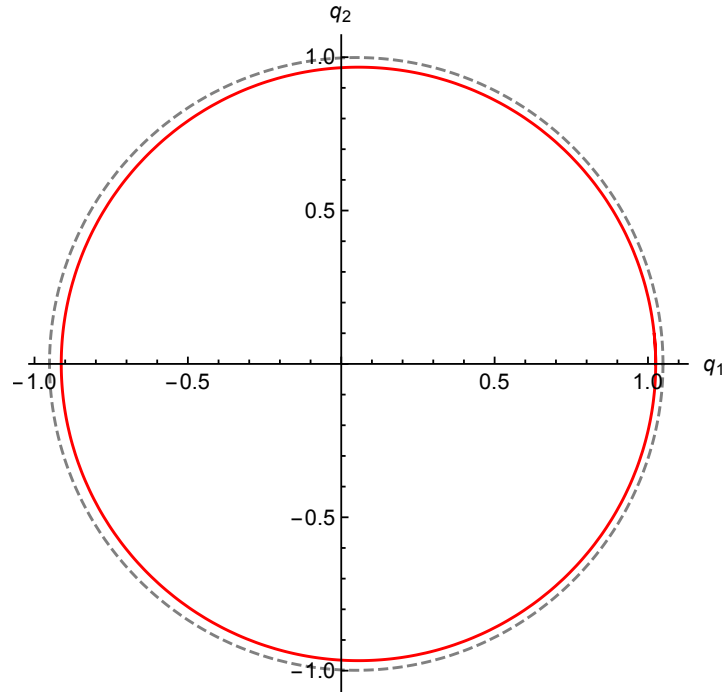


Figure 4.2: Jupiter's initial orbit (grey, dashed) and final orbit (red) are drawn in the  $(q_1, q_2)$  plane, showing the effects of the passing star. Jupiter's initial position is  $(q_1(-smax), q_2(-smax)) = (1.0489, 0)$ .

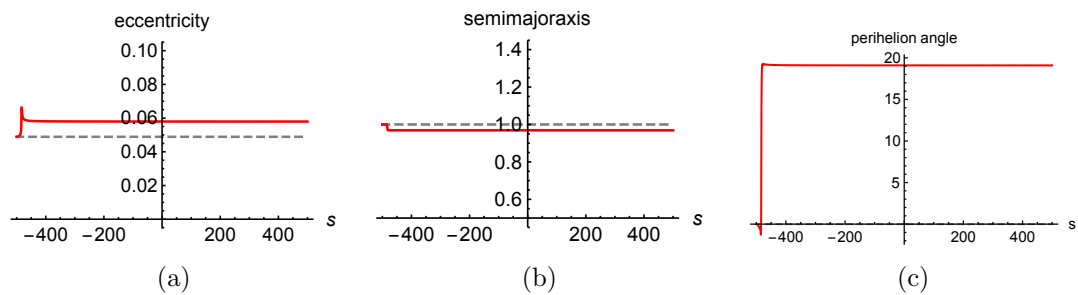


Figure 4.3: (a) The orbit of Jupiter's initial eccentricity (grey, dashed) and final eccentricity (red). (b) The orbit of Jupiter's initial semi-major axis (dashed, grey) and final semi-major axis (red). (c) The orbit of Jupiter's initial argument of the periastris (dashed, grey) and final argument of the periastris (red). In (a), (b) and (c), Jupiter's initial position is  $(q_1(-smax), q_2(-smax)) = (1.0489, 0)$ .

planet. The orbital period is given by

$$T_J = 2\pi \sqrt{\frac{a_J^3}{m_1}}.$$

For the initial value of  $a_J$ , the orbital period is 7.82391. The final value of the semi-major axis here is 0.9690063, yielding a shorter orbital period of 7.463.

The argument of the periapsis also changes as the star passes by. The argument of the periapsis is given by

$$\tan(\omega_J) = -\frac{e_{J_1}}{e_{J_2}}$$

where  $e = (e_{J_1}, e_{J_2})$ . That is,  $e_{J_1}$  and  $e_{J_2}$  make up the components of the eccentricity, or Laplace, vector. For the initial value of  $\omega_J$ , the argument of the periapsis is 0 degrees as the initial orbit begins with the major axis along the horizontal axis. The argument of the periapsis increases to  $19.1066^\circ$  (see figure 4.3c).

In the simulations featured in figure 4.2 and figure 4.3, the initial conditions of Jupiter's orbit were set to

$$(q_1(-\text{smax}), q_2(-\text{smax})) = (1.0489, 0).$$

This initial position informs where Jupiter is during the passing star's closest approach along the  $q_1$  axis. This can have an effect on how exactly Jupiter's orbit changes as the star passes. Starting at various points along Jupiter's initial orbit and running the simulation leads to different solutions. These solutions hold varying amounts of changes to the eccentricity, semi-major axis, period, and argument of the periapsis.

Table 4.3 details the the result of running the simulation for 16 different starting positions of Jupiter (see columns 1 and 2), equally distanced over the initial (current) orbit of Jupiter [58]. In the table, the various final values of eccentricity, along with the

$q_1(-\mathbf{smax})$	$q_2(-\mathbf{smax})$	$e_J(\mathbf{smax})$	% $\Delta a_J$	$T_J(\mathbf{smax})$	$\omega_J(\mathbf{smax})$
1.0489	0.0	0.0579576	-3.09937	7.463	19.1066
0.97278	0.382226	0.0542911	-3.40961	7.42719	23.2184
0.756007	0.706261	0.0486914	-3.16083	7.4559	23.5845
0.431583	0.922774	0.0446509	-2.41727	7.54194	18.9889
0.0489	0.998804	0.0448643	-1.30733	7.67098	12.4204
-0.333783	0.922774	0.0487823	-0.001156	7.82377	9.01296
-0.658207	0.706261	0.0534277	1.31278	7.97848	10.2666
-0.87498	0.382226	0.0562559	2.455	8.11378	14.5767
-0.9511	0.0	0.0561287	3.27651	8.21156	19.8478
-0.87498	-0.382226	0.0530516	3.66649	8.25812	24.2869
-0.658207	-0.706261	0.0481513	3.55609	8.24493	25.822
-0.333783	-0.922774	0.0437847	2.93012	8.17029	22.6209
0.0489	-0.998804	0.0430586	1.84818	8.0418	15.485
0.431583	-0.922774	0.0470903	0.463018	7.87831	9.94663
0.756007	-0.706261	0.0531985	-0.991304	7.70786	9.73182
0.97278	-0.382226	0.0575717	-2.25191	7.56112	13.6925

Table 4.3: Final value of eccentricity ( $e_J(\mathbf{smax})$ ), percentage change in the semi-major axis (%  $\Delta a_J$ ), final value of orbital period ( $T_J(\mathbf{smax})$ ), and the final value of the argument of the periapsis ( $\omega_J(\mathbf{smax})$ ) for the simulations with initial conditions found in the first two columns, along with those found in table 4.2. Recall that the initial value of  $e_J$  is 0.0489, the initial value for  $a_J$  is 1, the initial value of  $T_J$  is 7.82391, and the initial value of  $\omega_J$  is 0 degrees.

percent change of the semi-major axis, the new value of the period of the orbit, and the final argument of the periapsis, are listed. When the percent change of the semi-major axis is positive, the axis increased by this percent. Similarly, when the percent change of the semi-major axis is negative, this value decreased by this percent. Additionally, the argument of the periapsis is given in degrees.

Recall, from table 4.2, that the initial value of  $e_J$  is 0.0489 and the initial value for  $a_J$  is 1. In table 4.3, the eccentricity can be seen to both increase and decrease, with the most dramatic change being the jump to 0.0579576, with initial conditions

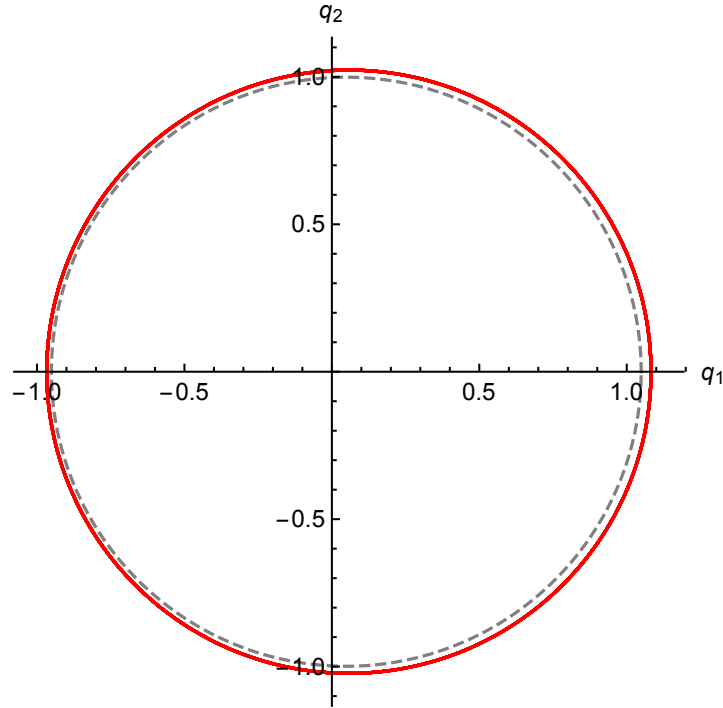


Figure 4.4: Jupiter's initial orbit (grey, dashed) and final orbit (red) are drawn in the  $(q_1, q_2)$  plane, showing the effects of the passing star. Jupiter's initial position is  $(q_1(-smax), q_2(-smax)) = (-0.87498, -0.382226)$ .

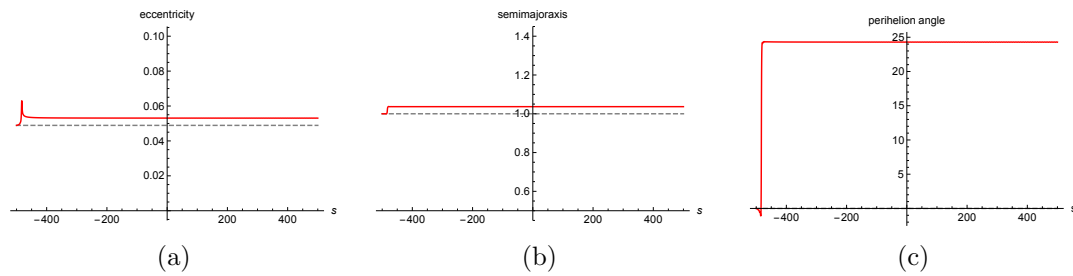


Figure 4.5: (a) The orbit of Jupiter's initial eccentricity (grey, dashed) and final eccentricity (red). (b) The orbit of Jupiter's initial semi-major axis (dashed, grey) and final semi-major axis (red). (c) The orbit of Jupiter's initial argument of the periastris (dashed, grey) and final argument of the periastris (red). In (a), (b) and (c), Jupiter's initial position is  $(q_1(-smax), q_2(-smax)) = (-0.87498, -0.382226)$ .



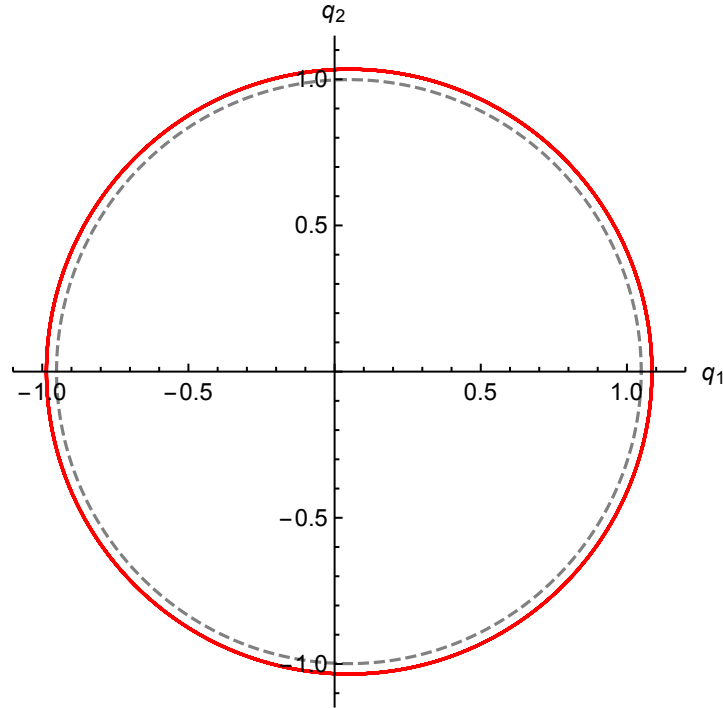


Figure 4.6: Jupiter's initial orbit (grey, dashed) and final orbit (red) are drawn in the  $(q_1, q_2)$  plane, showing the effects of the passing star. Jupiter's initial position is  $(q_1(-smax), q_2(-smax)) = (-0.658207, -0.706261)$ .

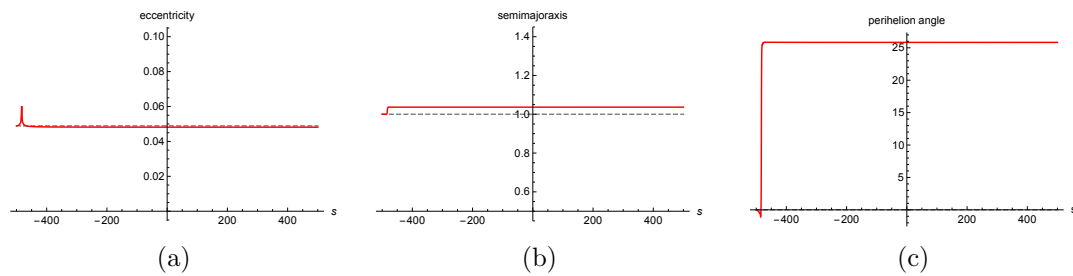


Figure 4.7: (a) The orbit of Jupiter's initial eccentricity (grey, dashed) and final eccentricity (red). (b) The orbit of Jupiter's initial semi-major axis (dashed, grey) and final semi-major axis (red). (c) The orbit of Jupiter's initial argument of the periastris (dashed, grey) and final argument of the periastris (red). In (a), (b) and (c), Jupiter's initial position is  $(q_1(-smax), q_2(-smax)) = (-0.658207, -0.706261)$ .

$(q_1(-\mathbf{smax}), q_2(-\mathbf{smax})) = (1.0489, 0.0)$  (see figure 4.2). The biggest change in the semi-major axis (and thus the biggest change in the orbital period) is found to be by an increase of 3.66649% in the case where the initial conditions are  $(q_1(-\mathbf{smax}), q_2(-\mathbf{smax})) = (-0.87498, -0.382226)$  (see figures 4.4 and 4.5). Though this does not correspond to the biggest change in the argument of the periapsis, it does correspond to the second largest change in the argument of the periapsis. The largest change in the argument of the periapsis occurs when  $(q_1(-\mathbf{smax}), q_2(-\mathbf{smax})) = (-0.658207, -0.706261)$  when the orbit rotates by almost  $26^\circ$  (see figures 4.6 and 4.7).

Not only do we observe several changes to the orbit of Jupiter here, it is important to note that this would have an effect on Earth's orbit as well as the secular fundamental frequencies would be affected. The changes in the argument of the periapsis in particular would have a strong effect on the  $g_i$  frequencies, the precession of the periapsis, as this would push these out of their regular oscillations.

### 4.3 Effects on the Orbit and Climate of Earth

As the Kuiper Belt is within the range of 1800 AU, a passing star of the size considered here will also have a direct effect on the orbit of Earth. Equation (2.24) is once again solved but with initial conditions related to Earth given by

$$z_1(\tau) = \frac{1}{\sqrt{2}} \sqrt{a_E(1+e_E)} \cos\left(\sqrt{\frac{m_1}{a_E}} \frac{\tau}{2}\right) \quad (4.10)$$

$$z_2(\tau) = \frac{1}{\sqrt{2}} \sqrt{a_E(1-e_E)} \sin\left(\sqrt{\frac{m_1}{a_E}} \frac{\tau}{2}\right) \quad (4.11)$$

$$w_1(\tau) = -\frac{1}{\sqrt{2}} \sqrt{\frac{m_1}{a_E}} \sqrt{a_E(1+e_E)} \sin\left(\sqrt{\frac{m_1}{a_E}} \frac{\tau}{2}\right) \quad (4.12)$$

$$w_2(\tau) = \frac{1}{\sqrt{2}} \sqrt{\frac{m_1}{a_E}} \sqrt{a_E(1-e_E)} \cos\left(\sqrt{\frac{m_1}{a_E}} \frac{\tau}{2}\right), \quad (4.13)$$

where

$$s = \frac{1}{2} \sqrt{\frac{m_1}{a_E}} \tau.$$

The values of  $a_E$  and  $e_E$  can be found in table 4.2, along with the all other parameters for this simulation. As the Earth is located closer to the Sun, the changes in the orbit are far less noticeable (see figure 4.8). In fact, the orbit does not even appear to change. This is not true of the semi-major axis, the eccentricity, and the argument of the periapsis however. The changes are small, but do exist for those orbital elements. The final value for the eccentricity of the orbit changes to 0.0176979 (see figure 4.9a), an increase of approximately 0.001. Additionally, the final value for the semi-major axis value is 0.192035, an increase of approximately 0.018% (see figure 4.9b). The change in the semi-major axis results in a change to the orbital period of the planet. For the initial value of  $a_E$ , the orbital period is 0.658227. The final value of the semi-major axis here yields a longer orbital period of 0.658406. Lastly, the final value of the argument of the periapsis is  $21.5522^\circ$ . Note that there is a bit of numerical error in the computation of the argument of the perihelion here.

In the simulations featured in figures 4.8 and 4.9, the initial conditions of Earth's orbit were set to

$$(q_1(-\mathbf{smax}), q_2(-\mathbf{smax})) = (0.195206, 0).$$

As in the previous section, the initial position of Earth informs how the orbit changes as the passing star approaches. The different solutions that come for the different initial conditions result in varying amounts of changes to the eccentricity and semi-major axis values. Table 4.4 details the result of running the simulation for 16 different starting positions of Earth (see columns 1 and 2), equally distanced over the initial (current) orbit of Earth [60].

The largest change in the eccentricity and semi-major axis are observed for the initial

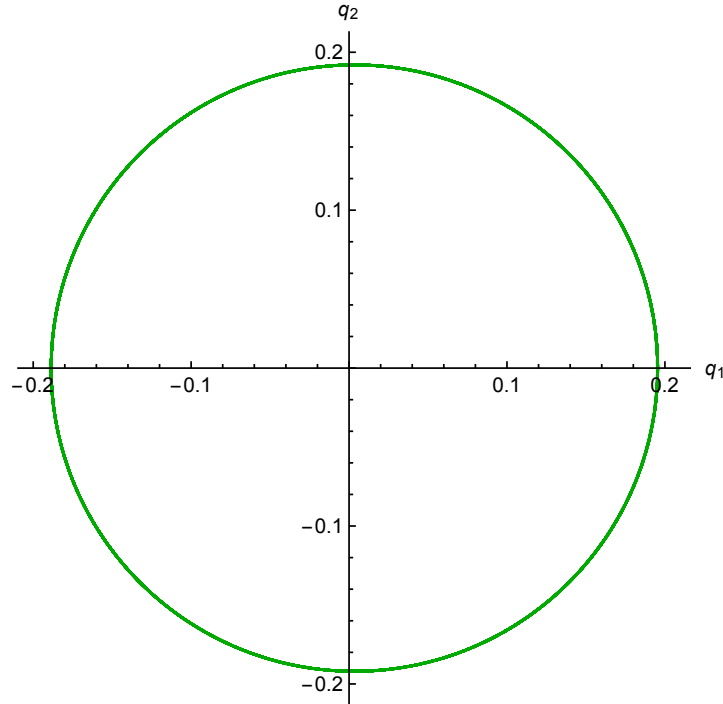


Figure 4.8: Earth's initial orbit (grey, dashed) and final orbit (green) are drawn in the  $(q_1, q_2)$  plane, showing the effects of the passing star. Earth's initial position is  $(q_1(-smax), q_2(-smax)) = (0.195206, 0)$ .

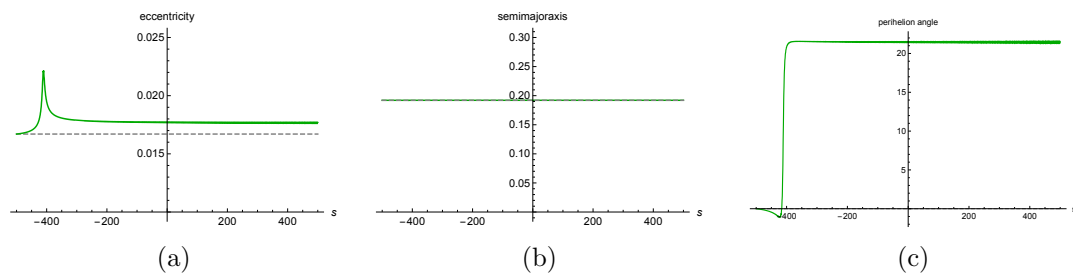


Figure 4.9: (a) The orbit of Earth's initial eccentricity (grey, dashed) and final eccentricity (green). (b) The orbit of Earth's initial semi-major axis (dashed, grey) and final semi-major axis (green). (c) The orbit of Earth's initial argument of the periastron (dashed, grey) and final argument of the periastron (green). In (a),(b) and (c), Earth's initial position is  $(q_1(-smax), q_2(-smax)) = (0.195206, 0)$ .

$q_1(-\mathbf{smax})$	$q_2(-\mathbf{smax})$	$e_E(\mathbf{smax})$	$\% \Delta a_E$	$T_E(\mathbf{smax})$	$\omega_E$
0.195206	0.0	0.0176979	0.0181964	0.658406	21.5522
0.180591	0.073465	0.017684	0.01408	0.658366	21.5898
0.138971	0.135746	0.0176666	0.00907275	0.658316	21.5946
0.0766816	0.17736	0.0176499	0.00423917	0.658268	21.5698
0.0032064	0.191973	0.0176366	$3.30223 \times 10^{-4}$	0.65823	21.5211
-0.0702688	0.17736	0.0176293	-0.00227686	0.658204	21.4563
-0.132558	0.135746	0.0176283	-0.00310203	0.658196	21.3892
-0.174178	0.073465	0.0176324	-0.00198253	0.658207	21.3292
-0.188794	0.0	0.0176411	$7.6627 \times 10^{-4}$	0.658234	21.284
-0.174178	-0.073465	0.0176526	0.00489697	0.658275	21.2561
-0.132558	-0.135746	0.0176661	0.00966544	0.658322	21.2502
-0.0702688	-0.17736	0.0176801	0.0144073	0.658369	21.2666
0.0032064	-0.191973	0.0176929	0.0184611	0.658409	21.3039
0.0766816	-0.17736	0.0177027	0.0211543	0.658435	21.3592
0.138971	-0.135746	0.0177077	0.0220829	0.658445	21.4258
0.180591	-0.073465	0.0177063	0.0210528	0.658434	21.4942

Table 4.4: Final value of eccentricity ( $e(\mathbf{smax})$ ), percentage change in the semi-major axis ( $\% \Delta a_E$ ), final value of orbital period ( $T_E(\mathbf{smax})$ ), and the final value of the argument of the periapsis ( $\omega_E(\mathbf{smax})$ ) for the simulations with initial conditions found in the first two columns, along with those found in table 4.2. Recall that the initial value of  $e_E$  is 0.0167, the initial value for  $a_E$  is 0.192, the initial value of  $T_E$  is 0.658227, and the initial value of  $\omega_E$  is 0 degrees.

conditions  $(q_1(-\mathbf{smax}), q_2(-\mathbf{smax})) = (0.180591, -0.073465)$  where  $e$  becomes 0.0177063 and the semi-major axis changes by approximately 0.022% (see figures 4.10 and 4.11). The largest change in the argument of the periapsis occurs when  $(-0.0702688, -0.17736)$  when the orbit rotates by  $21.2666^\circ$  (see figures 4.12 and 4.13).

Laskar et. al showed that the variations in the semi-major axis of Earth are so small that they will not create noticeable change in the average distance from the Earth to the Sun over the last 250 million years [32]. The values seen in table 4.4 are about ten times larger than those observed by Laskar et. al. in Earth's natural oscillations (see Figure 11 in [32]). This indicates that a star passing by the Kuiper Belt would cause a noticeable change to the semi-major axis.

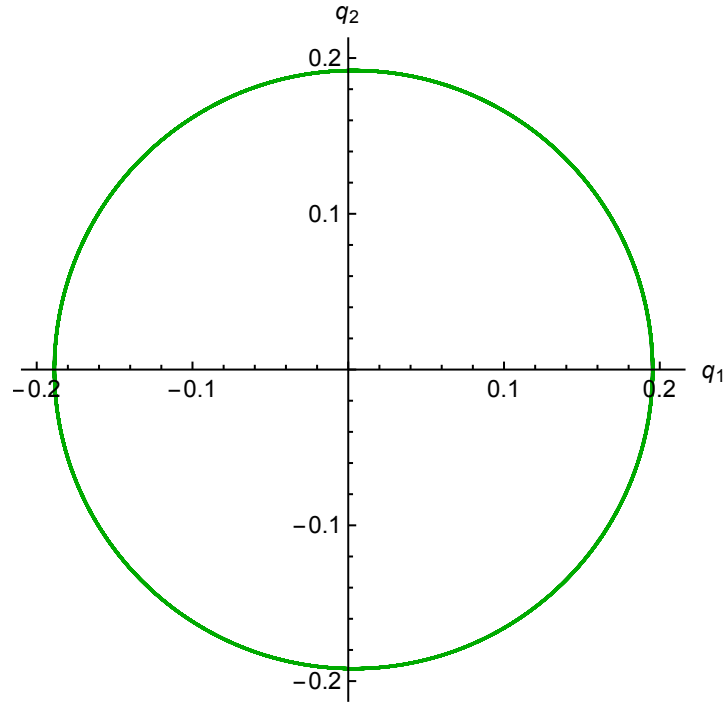


Figure 4.10: Earth's initial orbit (grey, dashed) and final orbit (green) are drawn in the  $(q_1, q_2)$  plane, showing the effects of the passing star. Earth's initial position is  $(q_1(-\text{smax}), q_2(-\text{smax})) = (0.180591, -0.073465)$ .

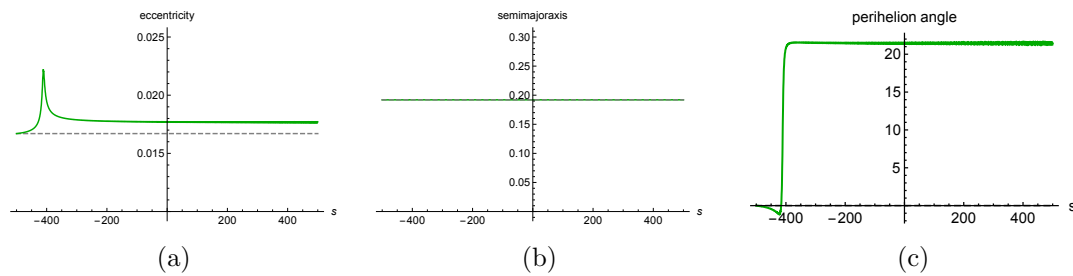


Figure 4.11: (a) The orbit of Earth's initial eccentricity (grey, dashed) and final eccentricity (green). (b) The orbit of Earth's initial semi-major axis (dashed, grey) and final semi-major axis (green). (c) The orbit of Earth's initial argument of the periaapsis (dashed, grey) and final argument of the periaapsis (green). In (a),(b) and (c), Earth's initial position is  $(q_1(-\text{smax}), q_2(-\text{smax})) = (0.138971, -0.135746)$ .

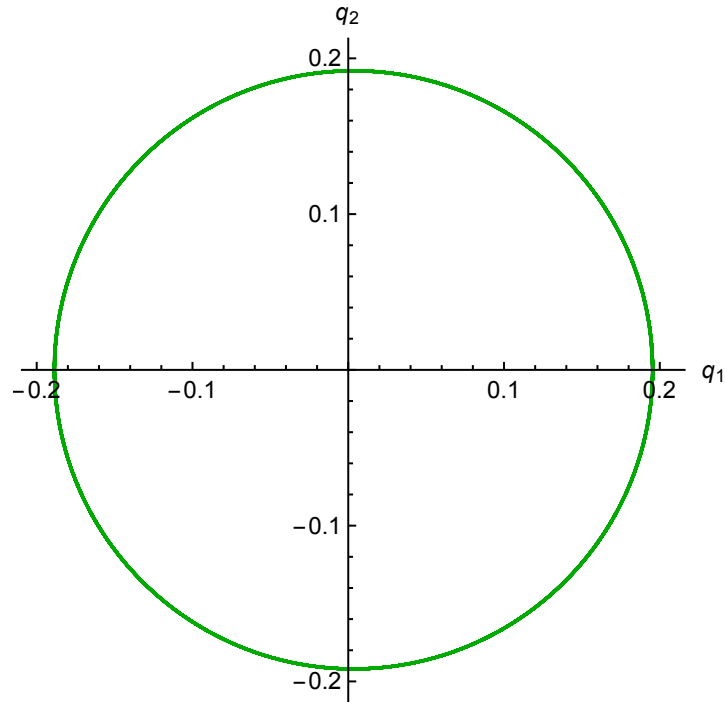


Figure 4.12: Earth's initial orbit (grey, dashed) and final orbit (green) are drawn in the  $(q_1, q_2)$  plane, showing the effects of the passing star. Earth's initial position is  $(q_1(-\text{smax}), q_2(-\text{smax})) = (-0.0702688, -0.17736)$ .

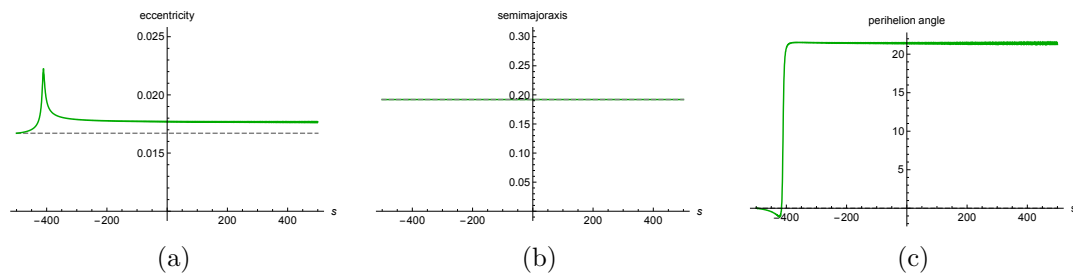


Figure 4.13: (a) The orbit of Earth's initial eccentricity (grey, dashed) and final eccentricity (green). (b) The orbit of Earth's initial semi-major axis (dashed, grey) and final semi-major axis (green). (c) The orbit of Earth's initial argument of the periapsis (dashed, grey) and final argument of the periapsis (green). In (a),(b) and (c), Earth's initial position is  $(q_1(-\text{smax}), q_2(-\text{smax})) = (-0.0702688, -0.17736)$ .

### 4.3.1 Global Mean Temperature Changes

Considering the changes that are made to the eccentricity and semi-major axis, it is worthwhile to consider the kinds of changes that would be observed in the temperature distribution from these specific changes. Using the Budyko-Widiasih model (see chapter 3), the global mean temperature will be plotted and analyzed.

The eccentricity of the Earth's orbit naturally oscillates from 0.00 to 0.06 on a 100,000 year cycle [32]. Oscillations observed in table 4.4 are within this range. These changes in the eccentricity have an effect on the global mean temperature, given by

$$\bar{T}^*(\eta) = \frac{Q(a_E, e_E) (1 - \bar{\alpha}(\eta)) - A}{B}, \quad (4.14)$$

where

$$\bar{\alpha}(\eta) = \alpha_{H_2O} \int_0^\eta s_6(y) dy + \alpha_{ice} \int_\eta^1 s_6(y) dy,$$

as it affects the incoming solar radiation. Let

$$\Delta GMT = \frac{Q(0, 0.0167) (1 - \bar{\alpha}(\eta)) - A}{B} - \frac{Q(a_E, e_E) (1 - \bar{\alpha}(\eta)) - A}{B}. \quad (4.15)$$

indicate the change in the global mean temperature from the current orbital parameter values. As the final values for the eccentricity found in table 4.4 do not leave the range of the regular oscillations of the Earth's eccentricity, the range of the eccentricities that Laskar et. al. gave are studied [32]. In figure 4.14, equation (4.15) is plotted with

$$e_E = 0, 0.02, 0.04, \text{ and } 0.06$$

and holding  $a_E = 1$ . Changes in these values range from the order of  $10^{-3}$  to  $10^{-1}$ . The changes are quite subtle around this range of differences. As such it can be assumed



that the changes for the values found in table 4.4 would be even more subtle, as those changes are in the range of 0.001 for the eccentricity.

The effects on the global mean temperature from changes to the semi-major axis are considered as well. Literature often assumes that the semi-major is constant, and the range over which it oscillates to be negligibly small. Consider instead the changes seen in table 4.4 as these changes are higher than those observed in [32]. In figure 4.15, equation (4.15) is plotted holding  $e_E = 0.0167$  and

$$a_E = 1.000220829, 1.0000966544, 0.9999801747, \text{ and } 0.999969\text{AU}.$$

Change here range on a smaller interval, closer to the order of  $10^{-2}$  or  $10^{-3}$ . These images suggest that changes in the semi-major axis ( $a_E$ ) have a stronger effect on the global mean temperature than changes to the eccentricity ( $e_E$ ). This is due to the fact that the global mean temperature changes resulting from changing  $a_E$  (figure 4.15) and those changes resulting from changes to the eccentricity  $e_E$  (figure 4.14) were on a similar scale for vertical axis, but not the horizontal.

### 4.3.2 Equilibrium Temperature Profile Changes

For the most dramatic change in  $a_E$  and  $e_E$  seen in Earth as the star passes in table 4.4, the equilibrium temperature profile changes can also be considered. Recall the equilibrium temperature profile from Budyko's model is given by equation (3.11). In figure 4.16, both the equilibrium temperature profile for Earth's current parameters and the most dramatic shift seen in Earth's parameters,  $a_E = 1.000220829$  AU and  $e_E = 0.0177077$ , are drawn. Only dramatic changes in the eccentricity and semi-major axis are considered here as these two have an effect in the Budyko-Widiasih model. Throughout the two temperature profiles, there is over a  $1^\circ\text{C}$  difference figure 4.16.

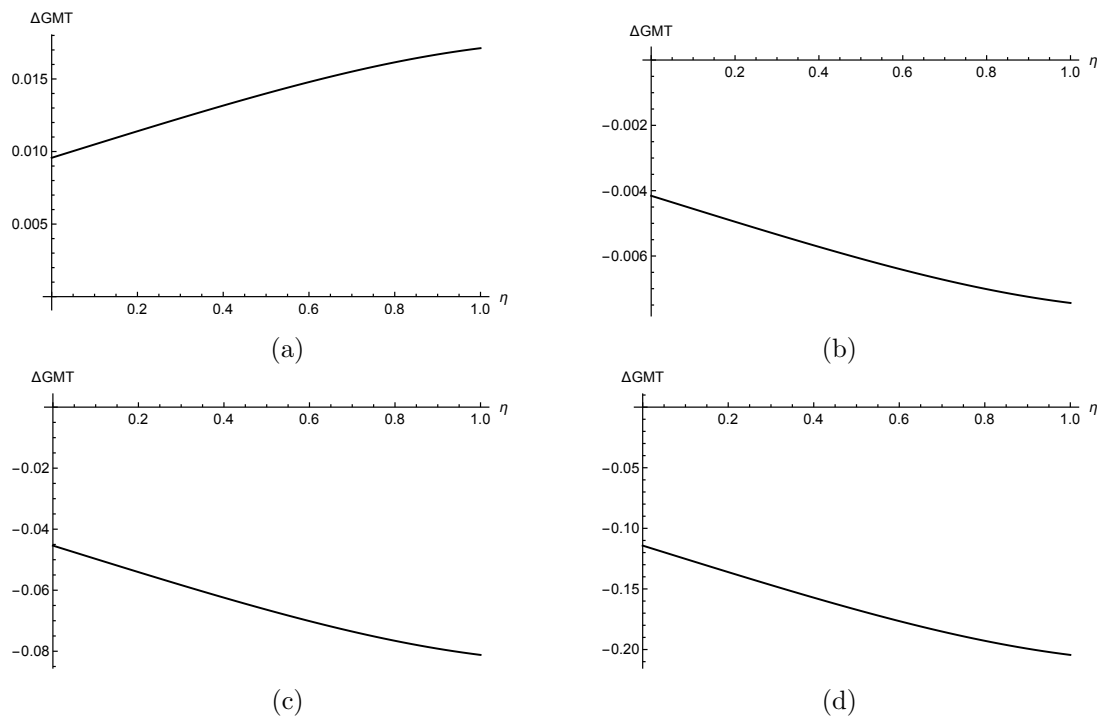


Figure 4.14: Change in global mean temperature as a function of the location of the ice line,  $\eta$ . Here  $\Delta GMT$  is the difference from the value of  $\bar{T}^*$  with Earth's current values minus the value of  $\bar{T}^*$  for various values of  $e_E$ . Semi-major axis held constant at 1 AU. (a) Eccentricity is  $e_E = 0$ . (b)  $e_E = 0.02$ . (c)  $e_E = 0.04$ . (d)  $e_E = 0.06$ .

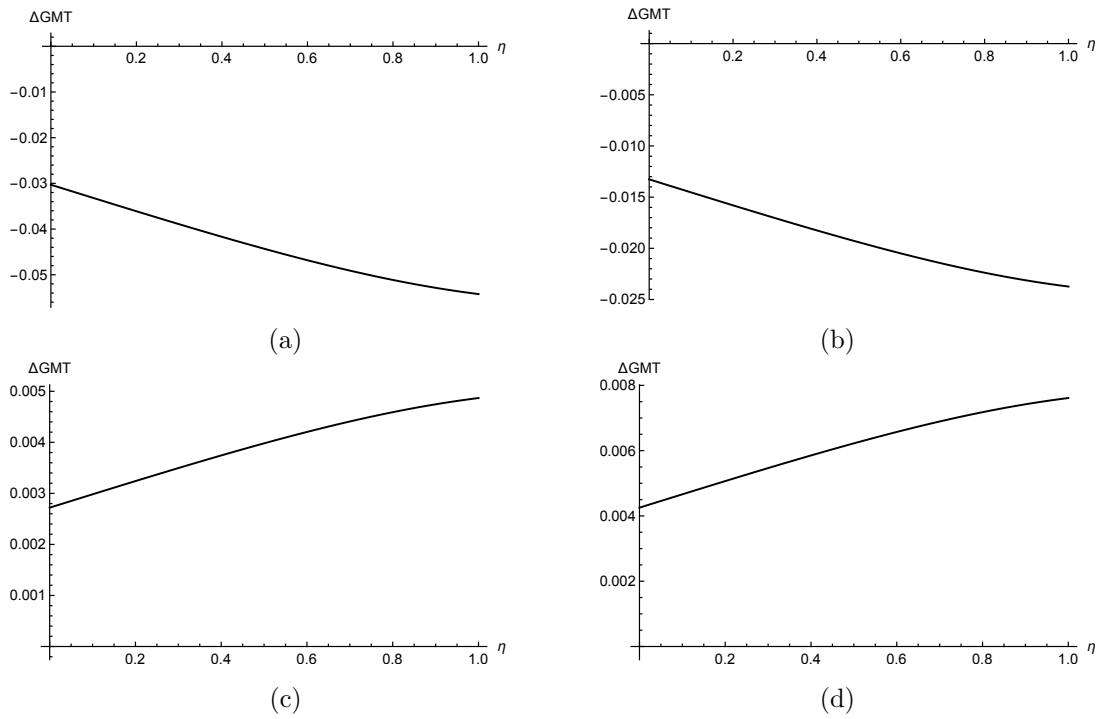


Figure 4.15: Change in global mean temperature as a function of the location of the ice line,  $\eta$ . Here  $\Delta GMT$  is the difference from the value of  $\bar{T}^*$  with Earth's current values minus the value of  $\bar{T}^*$  for various values of  $a_E$ . Eccentricity held constant at 0.0167. (a) Semi-major axis is  $a_E = 1.000220829$  AU. (b)  $a_E = 1.0000966544$  AU. (c)  $a_E = 0.9999801747$  AU. (d)  $a_E = 0.999969$  AU.

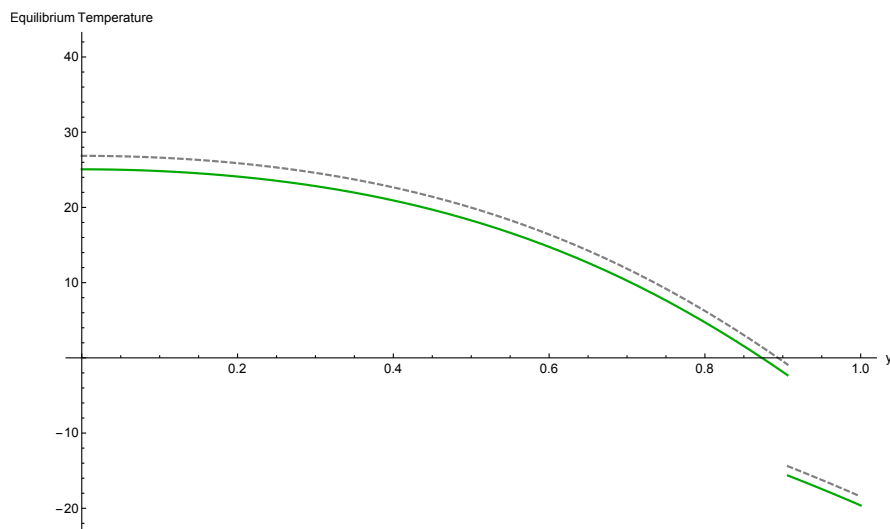


Figure 4.16: Earth’s current equilibrium temperature profile (grey, dashed) and equilibrium temperature profile when  $a = 1.000220829$  AU and  $e = 0.0177077$  (green). Temperature given in degrees Celsius. Ice line is located at  $66.5^\circ$  N.

This sort of change would be present in the sediment core data [44]. A cooling of  $1^\circ\text{C}$  is equivalent to a estimated  $\delta^{18}\text{O}$  increase of  $0.22\%$  [20]. This is an effect that would have wide ranging repercussions on Earth. Even a  $1^\circ\text{C}$  global change is significant because it takes an enormous amount of heat to warm all the oceans, atmosphere, and land by that much. In the past, a  $2$  to  $3^\circ\text{C}$  drop was plunged the Earth into the Little Ice Age [62]. A  $3$  to  $7^\circ\text{C}$  drop was enough to bury a large part of North America under ice during the Last Glacial Maximum [19]. The difference of  $1.79156^\circ\text{C}$  observed at the equator could be enough to dramatically change Earth’s climate.

### 4.3.3 Bifurcation Diagram in the Semi-Major Axis

The bifurcation diagram of the system with respect to the semi-major axis  $a$  is given in figure 4.17. The black curve is obtained by solving for the parameter  $a$  when  $T^*(\eta, t)$  is set to the critical temperature  $T_c$ . The large blue arrows indicate the dynamics of the ice line. If a pair of  $a$  and an initial ice line  $\eta$  is chosen to the right of the curve, then

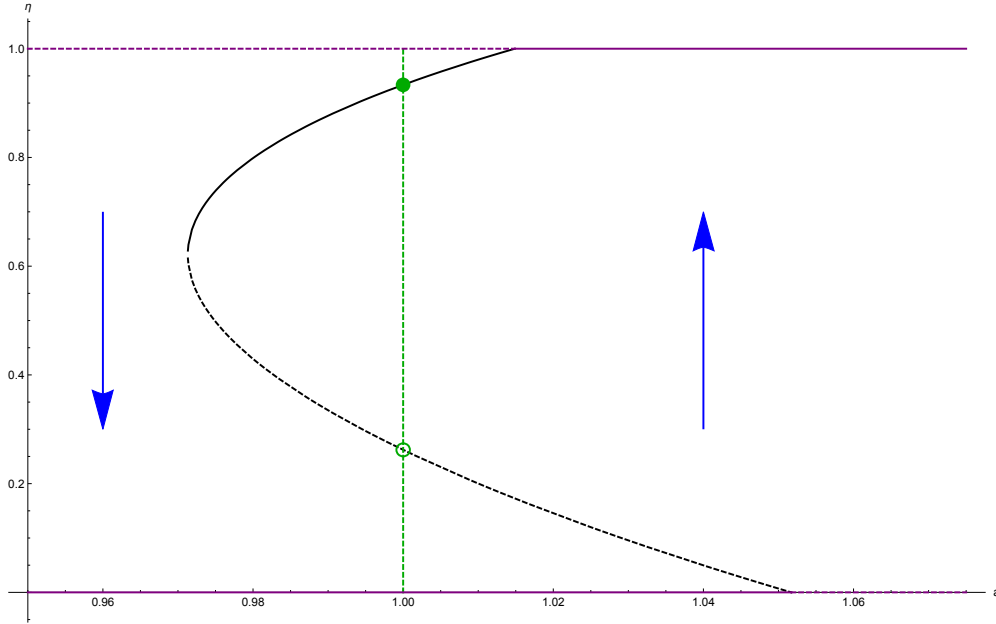


Figure 4.17: Bifurcation diagram of the semi-major axis  $a_E$ . Here  $e_E = 0.0167$ , the current value of Earth's eccentricity. All other parameters are in table 3.1. The current value of the Earth's semi-major axis is 1 and marked in green. The filled dot represents the stable equilibrium, and the open dot the unstable equilibrium.

the value of  $T^*(\eta, t)$  will be greater than the critical temperature  $T_c$ . In this case, the ice line equation dictates that the ice line moves up toward the pole; hence the upward blue arrow to the right of the black curve. In a similar fashion, choosing a combination left of the black curve will move the ice line toward the equator.

The value  $a = 1$  AU is highlighted in figure 4.17. With this value, there is an unstable big ice cap equilibrium at  $\eta \approx 0.262$  and a stable small ice cap equilibrium at  $\eta \approx 0.934$ . Furthermore, the stability of the branches above the saddle node bifurcation point for the values near  $a = 0.9713$  and  $\eta = 0.629$  is indicated by a solid black curve and the instability of the lower branch is represented by the dashed black curve.

There are also two bifurcation points when  $a \approx 1.0517$  (corresponding to  $\eta = 0$ ) and  $a \approx 1.0149$  (corresponding to  $\eta = 1$ ), where the determination of the bifurcation

type is less straightforward. The physically relevant condition that the ice line is not admissible outside of the unit interval gives a restriction on the dynamics of the ice line at the boundaries. That is [56],

$$\begin{aligned} \text{at the equator: } \eta = 0, \quad \frac{d\eta}{dt} &= \max \{0, \varepsilon (T(\eta, t) - T_c)\} \\ \text{at the pole: } \eta = 1, \quad \frac{d\eta}{dt} &= \min \{0, \varepsilon (T(\eta, t) - T_c)\}. \end{aligned}$$

This restriction determines the stability of the branches in the bifurcation diagram at the physical boundary. The purple solid lines in figure 4.17 at the equator suggests a ice covered planet (often referred to as “Snowball Earth”) whereas the solid line at the pole suggests an ice-free Earth. The purple dashed lines in the same figure indicate an unstable branch of the bifurcation diagram for  $a$ .

The stable equilibrium for Earth’s current semi-major axis value,  $a_E = 1$  AU, is when the ice line is located at  $68.9938^\circ$  N (filled green dot in figure 4.17). If the semi-major axis changes to  $a_E = 1.000220829$  AU, the ice line moves to  $69.1728^\circ$  N. Approximating Earth as a sphere, the surface area of ice lost here would be  $745790$  km<sup>2</sup>.

## 4.4 Discussion

In this chapter, the effects of a star passing at the edge of the Kuiper Belt on the orbits of Jupiter and Earth were studied. The initial position of the planet had an effect on the changes to the orbit that would be seen. If a star about half the size of the Sun were to pass by the edge of the Kuiper Belt, there would be noticeable changes to the orbital elements of Jupiter’s orbit, as can be observed from table 4.3, and subtler changes on the orbital elements of Earth’s orbit, as can be observed from table 4.4. The effects that these changes would have on the temperature distribution on Earth were also evaluated. The equilibrium temperature profile appears to move over  $1^\circ$  C, close to  $2^\circ$  C at many

points, which is a noticeable difference. Lastly, a bifurcation diagram was drawn to observe the way the semi-major axis length would affect the location of Earth's ice line.

In the case of Jupiter's orbit, there were some significant changes that occurred. The eccentricity, semi-major axis, and argument of the periapsis saw changes that would be visible in the sedimentary core data. While the range of the changes to eccentricity that were observed were within the natural oscillations of the eccentricity parameter, the semi-major axis changed at a rate higher than its natural oscillations [32]. This would surely disrupt the 400,000 year eccentricity cycle for planetary orbits. Additionally the changes to the argument of the periapsis would have an effect on the precession of the periapsis frequency, altering Jupiter's relationship to Earth.

In the case of Earth's orbit, without the compounding effects from the changes observed to Jupiter's orbit, the changes are quite small. There is still an effect on the equilibrium temperature profile, but the line does not significantly change, only moving  $0.2^\circ$  N even in the most dramatic of circumstances. This reveals that perhaps such an occurrence, without being able to account for the effects due to the changes of Jupiter, would not significantly contribute to glaciation or deglaciation. The biggest effects would be from the changes to the secular fundamental frequencies of Jupiter's orbit.

Given the changes observed to Jupiter's orbit, it can be safely assumed that a star of mass approximately half the size of the Sun did not pass within the Kuiper Belt during the last 65 million years as this would be observable in the climate record. The climate record prior to 65 million years ago has large gaps, but the work by Olsen et al. extending back to the Mesozoic era (250 to 65 million years ago) shows that the basic Milankovitch cycles were much of what we see today, indicating that a Kuiper Belt flyby probably has not occurred during the last 250 million years.

## Chapter 5

# Passage near the Oort Cloud

The distance that the passing star is in relation to the Sun and the planet will determine the kinds of effects that are observed. While marked differences in the orbits of Earth and Jupiter were observed in chapter 4 when the star passed by the edge of the Kuiper Belt, it begs the question: how far away the star can pass and still cause observable changes to orbits of planets in the Solar System?

The Oort cloud is a theoretical cloud of predominantly icy objects proposed to surround the Sun at distances ranging from approximately 3,000 to 50,000 AU <sup>1</sup> [57]. The Oort cloud lies beyond the heliosphere, in interstellar space. The Kuiper belt on the other hand is less than one thousandth as far from the Sun as the Oort cloud. The outer limit of the Oort cloud defines the boundary of the Solar System and the extent of the Sun's region of attraction, or Hill sphere. Unlike the orbits of the planets and the Kuiper Belt, which lie mostly in the same flat disk around the Sun, the Oort Cloud is believed to be a giant spherical shell surrounding the rest of the Solar System.

In chapter 4, it was shown that the Earth would be affected by a star passing within

---

<sup>1</sup>The bounds of the Oort cloud are not distinct and are often disputed. Some say it starts at 10,000 AU and some say it ends out at 100,000 AU. In this paper, 3,000 to 50,000 AU will be considered the Oort cloud.



approximately 1800 AU from the Sun. In this chapter, distances ranging from 100 AU all the way out to 50,000 AU will be considered for the closest approach of the passing star. The study will focus on the passing star's effects on Jupiter's orbit in this chapter as Earth cannot be affected alone at some of these more distant ranges. In section 1, the effect of the distance of the star on Jupiter's orbital elements is considered. Then in section 2, potential possible effects on the climate due to such changes are analyzed.

## 5.1 Varying Star's Distance with Constant Initial Position of the Planet

The distance of the star is controlled by the parameter  $a$ , the semi-major axis of the hyperbolic orbit of the star. By changing the position of the closest approach, the effect on the orbital elements as a result of the distance of the can be studied. Other parameters must be held constant, so all orbits will start along the horizontal axis at  $-s_{max}$ . Initial conditions remain similar as a result and can be found in table 5.1.

Parameter	Name	Value
$e$	eccentricity of orbit of passing star	2
$E$	hyperbolic anomaly of orbit of passing star	-3
$a_J$	semi-major axis of orbit of Jupiter	1
$e_J$	eccentricity of orbit of Jupiter	0.0489
$T_J$	period of Jupiter's orbit	7.82391
$\omega_J$	argument of the periapsis of Jupiter's orbit	0
$m_1$	mass of Sun	0.6449299
$m_2$	mass of passing star	0.3550701
$(z_1, z_2)$	initial position of Jupiter	(1.0489, 0.0)

Table 5.1: Initial conditions of the HR3BP for Jupiter as the third body in an elliptic orbit starting on the horizontal axis. The system has been scaled so that Jupiter could be a distance of 1 unit away.

As the star is moved further and further away, it makes sense that the effects on the orbit of Jupiter are diminishing. In figures 5.1 to 5.4, the orbit, eccentricity, semi-major axis, and argument of the periapsis of Jupiter are drawn from the values  $a = 100$  AU (figures 5.1 and 5.2a to 5.2c) and for  $a = 200$  AU (figures 5.3 and 5.4a to 5.4c). In figure 5.1, the initial and final orbit of Jupiter do not appear to change at all though the eccentricity and semi-major axis plots in figures 5.2a and 5.2b do show small changes that are still perceivable to the eye. Even in figure 5.4a, there is a small bump that can be seen near the beginning of the graph as the star passes. Notice additionally that the argument of the periapsis graph is accumulating more error as the value of  $a$  increases, making it a less reliable metric.

These effects are summarized in table 5.2. Around 1000 AU, the star's effect particularly appears to drop off. Though the changes have all been small, there is a noticeable change in the order of the percent change in the semi-major axis of the orbit of Jupiter between the star's closest approach being at 750 AU versus at 1000 AU.

After  $a = 30000$  AU, the value of the eccentricity of Jupiter's orbit appears constant, as do the period of Jupiter's orbit. While the value  $a_J$  appears to continue changing, the value is so small that it has no effect on  $T_J$ . After  $a = 30000$  AU, the value of  $\omega_J$  stays constant for four decimal places. Table 5.2 implies that after 30000 AU, the effects of the passing star are imperceptible. Though it appears that changes are still happening, these minuscule changes can be the result of numerical error. This means that subtle changes on the orbit of Jupiter due to a passing star may still be present so long as the star passes within approximately 30000 AU. While there are still subtle changes happening around  $a = 20000$  AU and  $a = 10000$  AU, those changes are also quite small and could be very difficult to notice in the geological record.

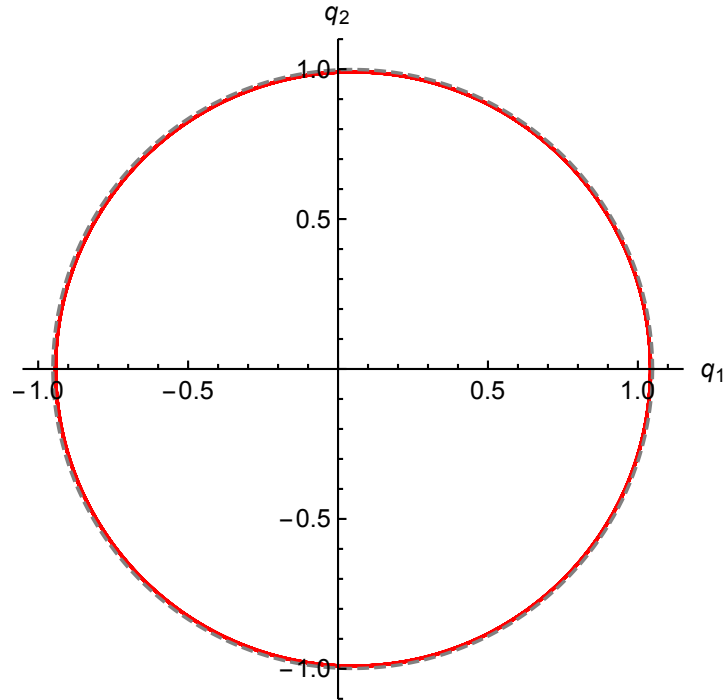


Figure 5.1: Jupiter's initial orbit (grey, dashed) and final orbit (red) are drawn in the  $(q_1, q_2)$  plane, showing the effects of the passing star. The star's closest approach is at 100 AU.

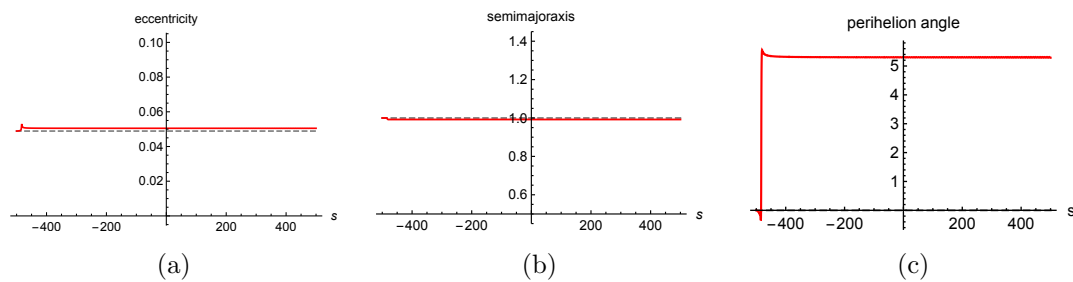


Figure 5.2: (a) The orbit of Jupiter's initial eccentricity (grey, dashed) and final eccentricity (red). (b) The orbit of Jupiter's initial semi-major axis (dashed, grey) and final semi-major axis (red). (c) The orbit of Jupiter's initial argument of the periastron (dashed, grey) and final argument of the periastron (red). In (a),(b) and (c), the star's closest approach occurs at 100 AU.

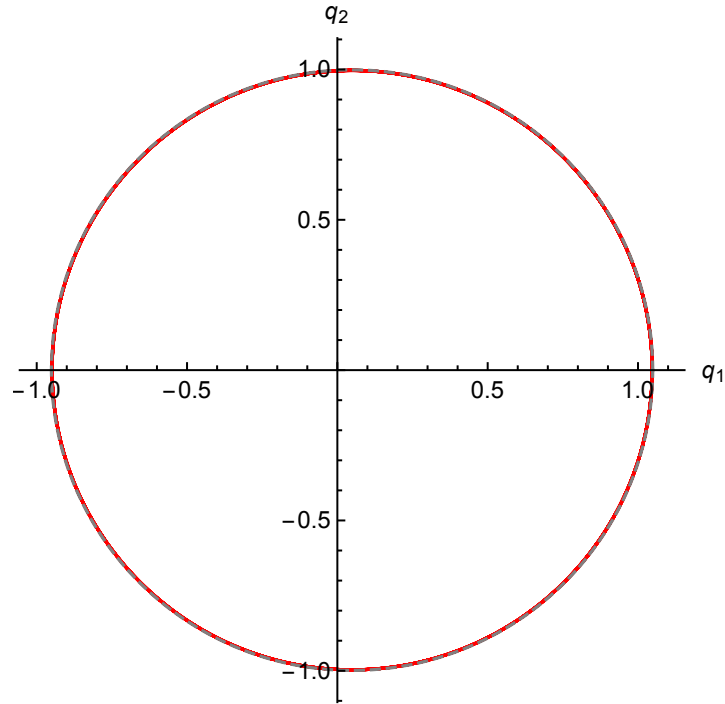


Figure 5.3: Jupiter's initial orbit (grey, dashed) and final orbit (red) are drawn in the  $(q_1, q_2)$  plane, showing the effects of the passing star. The star's closest approach is at 200 AU.

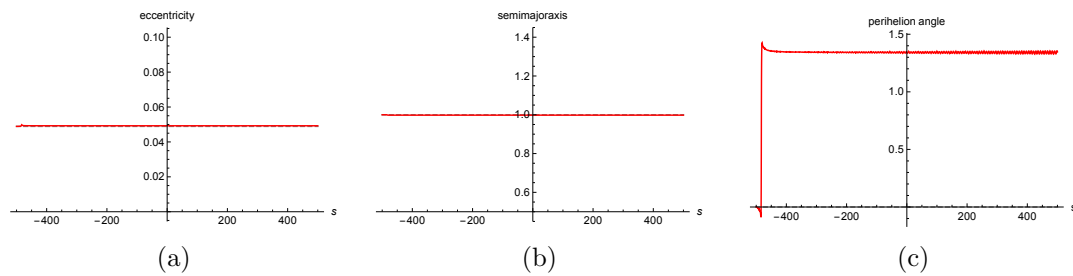


Figure 5.4: (a) The orbit of Jupiter's initial eccentricity (grey, dashed) and final eccentricity (red). (b) The orbit of Jupiter's initial semi-major axis (dashed, grey) and final semi-major axis (red). (c) The orbit of Jupiter's initial argument of the periastron (dashed, grey) and final argument of the periastron (red). In (a),(b) and (c), the star's closest approach occurs at 200 AU.

$a$	$e_J(\mathbf{smax})$	$\% \Delta a_J$	$T_J(\mathbf{smax})$	$\omega_J(\mathbf{smax})$
100	0.0505012	-0.775703	7.73305	5.28593
200	0.0492389	-0.191121	7.80149	1.34754
300	0.0490427	-0.0833261	7.81413	0.606828
400	0.0489771	-0.0457074	7.81854	0.347067
500	0.0489473	-0.0283277	7.82058	0.226833
750	0.0489182	-0.0111906	7.82259	0.108161
1000	0.0489081	-0.00520196	7.8233	0.0666694
2000	0.0488984	0.000564855	7.8239	0.0267012
3000	0.0488966	0.0016314	7.8241	0.0193084
4000	0.048896	0.00200461	7.82414	0.0167222
5000	0.0488957	0.00217728	7.82416	0.0155255
7500	0.0488954	0.00234748	7.82418	0.0143421
10000	0.0488953	0.00240714	7.82419	0.0139286
20000	0.0488952	0.00246467	7.82419	0.0135299
30000	0.0488952	0.00247562	7.8242	0.0134578
40000	0.0488952	0.00247935	7.8242	0.0134319
50000	0.0488952	0.0024807	7.8242	0.0134183
100000	0.0488952	0.00248307	7.8242	0.0134024

Table 5.2: Final value of eccentricity ( $e_J(\mathbf{smax})$ ), percentage change in the semi-major axis ( $\% \Delta a_J$ ), final value of orbital period ( $T_J(\mathbf{smax})$ ), and final value of the argument of the periapsis ( $\omega_J(\mathbf{smax})$ ) for the simulations with distance of closest approach given by the first column,  $a$ , along with those found in table 5.1. Recall that the initial value of  $e_J$  is 0.0489, the initial value for  $a_J$  is 1, the initial value of  $T_J$  is 7.82391, and the initial value of  $\omega_J$  is 0 degrees.

### 5.1.1 Global Mean Temperature Changes

To study more closely if effects of a distant passing star could be noticeable in the climate record, the global mean temperature is be plotted. As the parameters for the Budyko model are known for Earth, the assumption will be made that the changes observed to Jupiter will occur at the same percentage to Earth. For example, consider the case of  $a = 100$  AU for the closest approach of the star. For  $e_J = 0.0505012$ , meaning that the eccentricity of Jupiter's orbit has increased by approximately 3.27%. Additionally, it is known that a decreased by 0.775703%. Thus,  $e_E$  will be increased by the same

percentage and  $e_E \approx 0.017247$  and  $a_E$  will be decrease by the same amount yielding  $a_E = 0.99224297$  AU. These new values are plugged into equation (4.14).

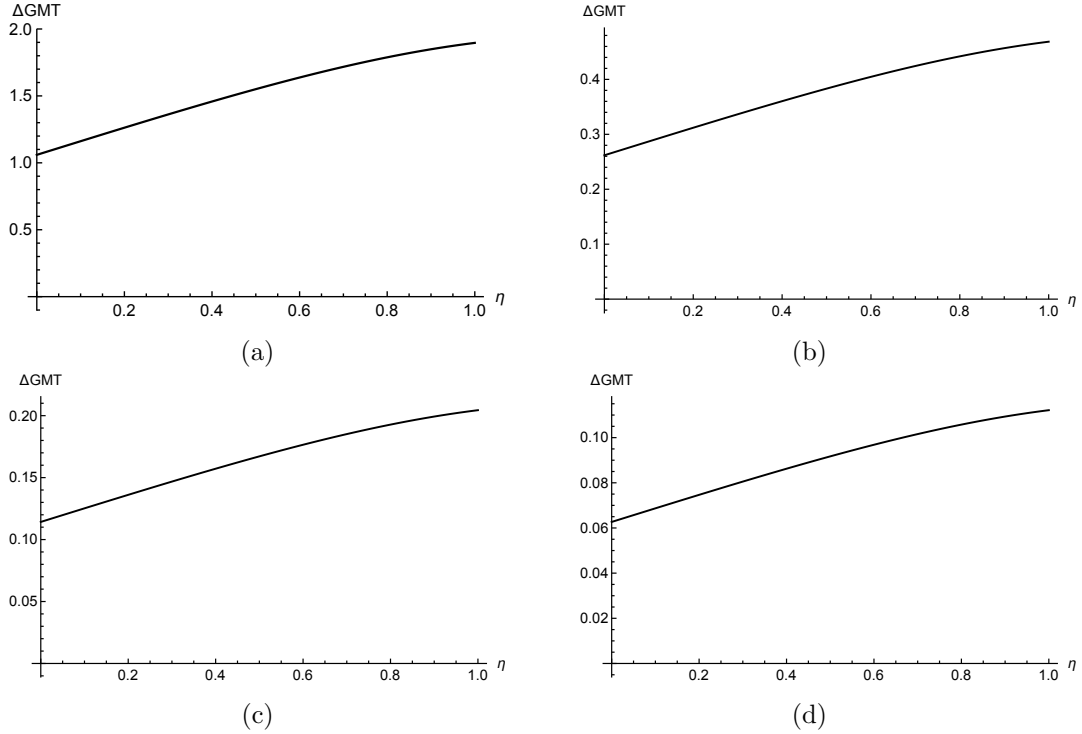


Figure 5.5: Change in global mean temperature as a function of the location of the ice line,  $\eta$  based off the values found in table 5.2. Here  $\Delta GMT$  is the difference from the value of  $\bar{T}^*$  with Earth's current values minus the value of  $\bar{T}^*$  for various values of  $a_E$ . (a)  $a = 100$  AU; (b)  $a = 200$  AU; (c)  $a = 300$  AU; (d)  $a = 400$  AU.

In figure 5.5, the change in global mean temperature is plotted (see equation (4.15)) for the closest approach of the star being  $a = 100$  AU (figure 5.5a),  $a = 200$  AU (figure 5.5b),  $a = 300$  AU (figure 5.5c), and  $a = 400$  AU (figure 5.5d).

For the case of  $a = 100$  in figure 5.5a, there is a marked difference between the global mean temperature for Earth's current orbital elements versus the orbital elements after the star passes. If the ice line were at the equator ( $\eta = 0$ ), the global mean temperature would decrease by  $0.896963^\circ\text{C}$  and if the ice line were at the pole ( $\eta = 1$ ), the global

mean temperature would decrease by  $1.60509^{\circ}\text{C}$ . For the case of  $a = 200$  in figure 5.5b, the biggest difference between the two graphs is  $0.468609^{\circ}\text{C}$  at the pole. In figure 5.5d for  $a = 400$  AU has a difference of  $0.112154^{\circ}\text{C}$  for the global mean temperature if the ice line were at the pole.

	$a = 100$	$a = 500$	$a = 1000$	$a = 5000$	$a = 10000$
$\Delta \text{ GMT}(0.0)$	1.05965	0.0388468	0.00713469	-0.00298598	-0.00330124
$\Delta \text{ GMT}(0.2)$	1.26244	0.0462811	0.0085001	-0.00355742	-0.00393302
$\Delta \text{ GMT}(0.4)$	1.45808	0.0534533	0.00981736	-0.00410872	-0.00454252
$\Delta \text{ GMT}(0.6)$	1.63743	0.0600283	0.0110249	-0.0046141	-0.00510126
$\Delta \text{ GMT}(0.8)$	1.7883	0.0655591	0.0120407	-0.00503923	-0.00557128
$\Delta \text{ GMT}(1.0)$	1.89622	0.0695153	0.0127673	-0.00534333	-0.00590748

Table 5.3: The difference between the global mean temperature (GMT) before the star passes to after the star passes at various ice line locations and for various closest approaches of the star. If the number is negative, the global mean temperature increases after the star passes, and if it is positive, the global mean temperature decreases after the star passes.

Table 5.3 lists values of equation (4.15) at various ice line locations and for various closest approaches of the star where the columns designate the distance of the closest approach of the passing star. Even when the star is 10000 AU away, there are still minute changes occurring in the global mean temperature profile. For  $a = 5000$  AU and  $a = 10000$  AU, the global mean temperature appears to increase slightly whereas for the smaller values of  $a$  the global mean temperature decreased. This is due to the fact that starting with  $a = 2000$  AU, the value of the semi-major axis increases slightly when the star passes (as can be seen in table 5.2). As was previously noted, in particular the changes are quite minor when the star approaches further away than 1000 AU as all changes occur on an order of  $10^{-3}$ .

### 5.1.2 Equilibrium Temperature Profile Changes

As there are notable changes to the global mean temperature when the star passes at 100 AUs as its closest approach, the equilibrium temperature profile will be drawn for this case. Recall that the equilibrium temperature profile is given by equation (3.11). In this case, the semi-major axis shrinks and the eccentricity increases.

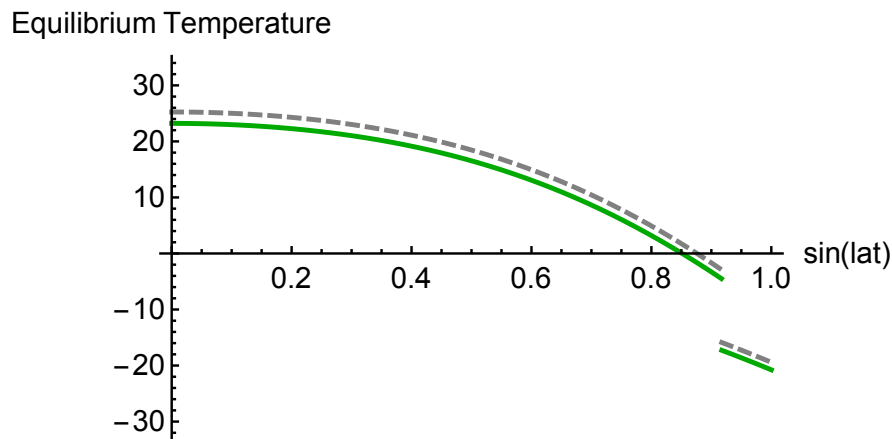


Figure 5.6: Earth’s current equilibrium temperature profile (grey, dashed) and equilibrium temperature profile when  $a_E = 0.99224297$  AU and  $e_E \approx 0.0172468$  (green) which occurs when the closest approach is at  $a = 100$  AUs. Temperature given in degrees Celsius. Ice line is located at  $66.5^\circ$  N here.

The equilibrium temperature profile given in figure 5.6 differs by over  $2^\circ\text{C}$  at the equator ( $\eta = 0$ ) and by around  $1.3^\circ\text{C}$  at the pole ( $\eta = 1$ ). This is a dramatic enough change to the the temperature profile that it would be spotted in the climate data.

## 5.2 Varying the Initial Position of the Planet

As seen from chapter 4, the initial position of Jupiter can have a significant effect on the way that the way the orbital elements change as the rogue star passes. In this section, the initial position of the planet will be varied along with the closest approach of the passing star. The closest approach of the star was varied from  $a = 100$  AU to  $a = 1000$



AU and the orbit of Jupiter was split into 100 equally spaced starting points. The starting position of Jupiter which resulted in the largest variation in either eccentricity, semi-major axis, and the argument of the periapsis is listed in tables 5.4 to 5.6.

Table 5.4 holds the initial conditions at which the eccentricity showed the greatest variation for the case of  $a$  found in the first column. Similarly, table 5.5 does this for the greatest variation of the semi-major axis (in absolute deviation) and table 5.6 does this for the greatest variation of the argument of the perihelion. While the largest variation in the eccentricity is approximately 0.0001 larger than the eccentricity variation found in table 5.2, the largest variation in the argument of the periapsis is over  $1^\circ$  larger and the largest variation in the semi-major axis changes by over 0.1%. The change in the argument of the periapsis in particular is the most interesting as this would change Jupiter's resonance with Earth, having an effect on the orbit and climate.

### 5.2.1 Global Mean Temperature Changes

The global mean temperature is considered for the changes in tables 5.4 and 5.5 as the eccentricity and the semi-major axis length contribute to the incoming solar radiation. Once again, as the parameters for the Budyko-Widiasih model are known for Earth, the changes observed are assumed to happen in the same percentage. In figure 5.7, changes in the global mean temperature are drawn for the first three rows of table 5.4 where  $a = 100, 200,$  and  $300$  AU. In figure 5.8, changes in the global mean temperature are drawn for the first three rows of table 5.5 where  $a = 100, 200,$  and  $300$  AU.

In figures 5.7 and 5.8, the global mean temperatures move with the value of the semi-major axis. When the semi-major axis increases, the global mean temperature profile increases whereas when the semi-major axis decreases, the global mean temperature profile decreases. The biggest change occurs in figure 5.8a, where the star passes at  $a = 100$  AU and the largest change is in the semi-major axis and the argument of the

$a$	$(q_1(-\text{smax}), q_2(-\text{smax}))$	$e_J(\text{smax})$	$\% \Delta a_J$	$T_J(\text{smax})$	$\omega_J(\text{smax})$
100	(1.01748, -0.248392)	0.0507187	-0.6462	7.7481910	4.30786
200	(0.999957, -0.308647)	0.0493079	-0.148068	7.80653488	1.03733
300	(0.999957, -0.308647)	0.0490767	-0.0640961	7.81638448	0.46893
400	(0.999957, -0.308647)	0.048998	-0.0348672	7.81981389	0.269818
500	(0.999957, -0.308647)	0.048962	-0.0213799	7.82139652	0.177741
750	(-0.902157, 0.308647)	0.0489279	0.0145121	7.825608682	0.068049
1000	(-0.933387, 0.187157)	0.0489166	0.00994914	7.825073147	0.0367391

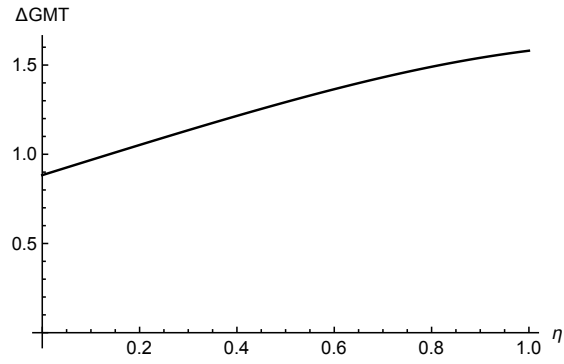
Table 5.4: Orbital elements after the star passes from varying distances (closest approach of star given in column 1). The starting locations (column 2) that resulted in the largest changes in the eccentricity are given.

$a$	$(q_1(-\text{smax}), q_2(-\text{smax}))$	$e_J(\text{smax})$	$\% \Delta a_J$	$T_J(\text{smax})$	$\omega_J(\text{smax})$
100	(-0.855927, -0.42527)	0.0489522	0.895905	7.9292828	6.38302
200	(-0.855927, -0.42527)	0.0488604	0.224227	7.8502352	1.57297
300	(-0.855927, -0.42527)	0.048884	0.100982	7.83575960	0.691083
400	(-0.855927, -0.42527)	0.0488946	0.0579254	7.83070453	0.383763
500	(-0.855927, -0.42527)	0.0488999	0.0380126	7.82836703	0.241752
750	(-0.855927, -0.42527)	0.0489053	0.0183561	7.826059846	0.101644
1000	(-0.855927, -0.42527)	0.0489073	0.0114788	7.825252675	0.0526429

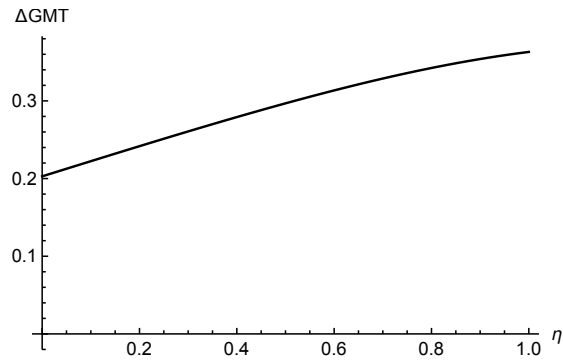
Table 5.5: Orbital elements after the star passes from varying distances (closest approach of star given in column 1). The starting locations (column 2) that resulted in the largest changes in the semi-major axis are given.

$a$	$(q_1(-\text{smax}), q_2(-\text{smax}))$	$e_J(\text{smax})$	$\% \Delta a_J$	$T_J(\text{smax})$	$\omega_J(\text{smax})$
100	(-0.827407, -0.481177)	0.0487435	0.894821	7.9291550	6.402
200	(0.925207, 0.481177)	0.0488555	-0.218216	7.7983100	1.58209
300	(0.925207, 0.481177)	0.0488688	-0.0957713	7.81266861	0.708449
400	(0.953727, 0.42527)	0.0488917	-0.0527492	7.81771575	0.402492
500	(0.953727, 0.42527)	0.0488911	-0.0328775	7.82004736	0.261065
750	(0.953727, 0.42527)	0.0488909	-0.0132791	7.822347136	0.121253
1000	(0.978676, 0.367684)	0.0488937	-0.00635297	7.823159937	0.072523

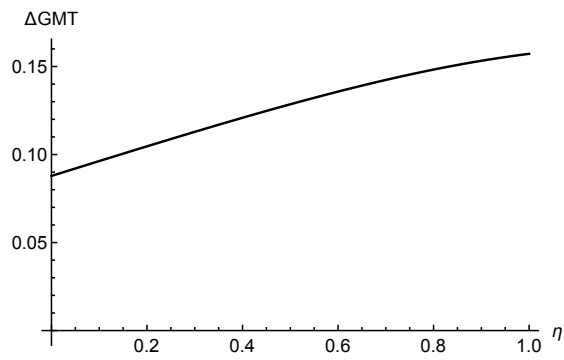
Table 5.6: Orbital elements after the star passes from varying distances (closest approach of star given in column 1). The starting locations (column 2) that resulted in the largest changes in the argument of the periapsis are given.



(a)

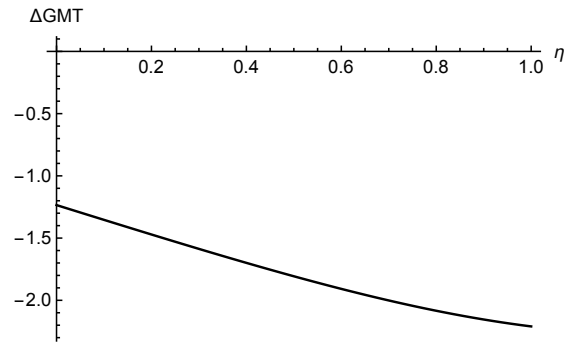


(b)

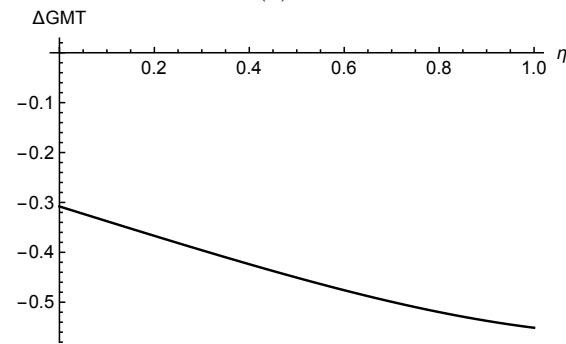


(c)

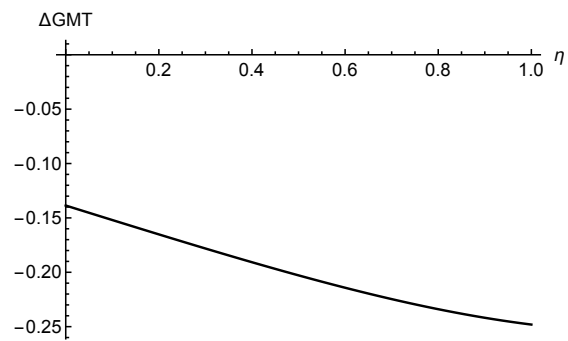
Figure 5.7: Change in global mean temperature as a function of the location of the ice line,  $\eta$  based off the values found in table 5.4. Here  $\Delta GMT$  is the difference from the value of  $\bar{T}^*$  with Earth's current values minus the value of  $\bar{T}^*$ . (a) (1.01748, -0.248392), (b) (0.999957, -0.308647), (c) (0.999957, -0.308647).



(a)



(b)



(c)

Figure 5.8: Change in global mean temperature as a function of the location of the ice line,  $\eta$  based off the values found in table 5.4. Here  $\Delta GMT$  is the difference from the value of  $\bar{T}^*$  with Earth's current values minus the value of  $\bar{T}^*$ . (a)  $(-0.855927, -0.42527)$ , (b)  $(-0.855927, -0.42527)$ , (c)  $(-0.855927, -0.42527)$

periapsis. The semi-major axis changes continue to have a strong effect on the global mean temperature. While the argument of the periapsis does not come into play in equation (4.14), it affects the resonances in the Solar System.

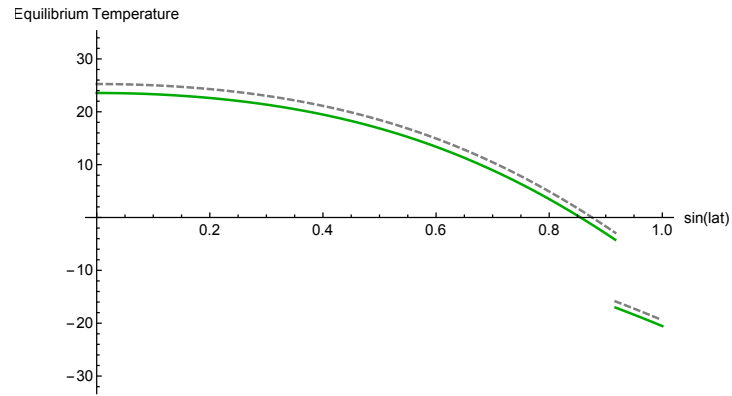
### 5.2.2 Equilibrium Temperature Profile Changes

For the global mean temperature profiles studied in the previous section where  $a = 100$  AU for the closest approach of the passing star, the equilibrium temperature profiles are plotted. Figure 5.9a is for the case of the biggest change in the eccentricity and figure 5.9b is for the case of the biggest change in the semi-major axis.

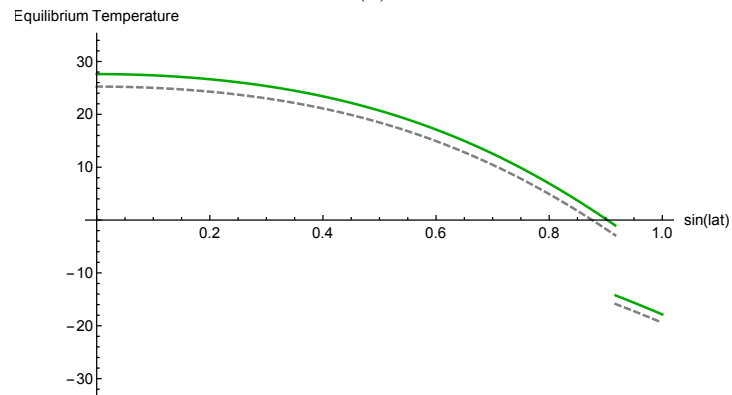
In all the curves of figure 5.9, the dashed, grey curve denotes the equilibrium temperature profile for Earth's current orbital elements with  $a_E = 1$  AU and  $e_E = 0.0167$ . In figure 5.9a,  $a = 100$  AU for the initial condition  $(1.01748, -0.248392)$ . The two profiles differ by over  $1.5^\circ$  C, with a maximum difference of approximately  $2.4^\circ$  C when  $\eta = 0$ . Figure 5.9b has a difference of around  $1.1^\circ$  C -  $1.7^\circ$  C in the equilibrium temperature profile with Earth's current orbit.

## 5.3 Discussion

In this chapter, the sensitivity of the Sun-planet-star system to the distance of the star's closest approach was analyzed. First, the effects on the orbital elements were noted, followed by the possible effects those could have on Earth's climate. As the passing star moves further away from the Solar System, the perturbing effects on Jupiter's orbit are weakened, as expected. When the star's closest approach is around 1000 AU, the effect particularly appears to drop off as the order of the percent change in the semi-major axis changes at this point. The semi-major axis is of particular note as it has the strongest influence on the global mean temperature and equilibrium temperature



(a)



(b)

Figure 5.9: Earth's current equilibrium temperature profile (grey, dashed) and equilibrium temperature profile when (a)  $(1.01748, -0.248392)$ ,  $a = 100$  AU, biggest change in eccentricity; (b)  $(-0.855927, -0.42527)$ ,  $a = 100$  AU, biggest change in semi-major axis. Temperature given in degrees Celsius. Ice line is located at  $66.5^\circ$  N here.

profiles of the planet. The changes in the argument of the periapsis are very minimal at these distances, shifting at most approximately  $5^\circ - 6^\circ$ .

Different starting points were also considered. A smaller range of the closest approach was considered here as opposed to the earlier section as it was previously noted that 1000 AU is where there appears to be a drop off in the effect of the passing star. Larger effects by the passing star were observed at various starting locations. The changes in the semi-major axis continued to have the largest effect on the planet's temperature profile. Some of the changes observed in this chapter could have a  $1^\circ \text{ C}$  to  $2^\circ \text{ C}$  change in the temperature profile, a significant change as noted in chapter 4.

As the parameters for the Budyko-Widiasih model that are known are for Earth, the study of the climate in this chapter was based off assumptions of how the Earth's orbits might change as a result of Jupiter's orbit. It did not take into direct account the effects of the secular fundamental frequencies but instead considered that case of the same percentage changes happening to Earth's orbit that happened to Jupiter's. The global mean temperature profile had changes ranging from  $2^\circ \text{ C}$  for the case of  $a = 100$  AU to around  $0.1^\circ \text{ C}$  when the star passes at  $a = 300$  AU from the Sun. Equilibrium temperature profiles shifted by around  $1^\circ \text{ C} - 2^\circ \text{ C}$  in the most dramatic cases when  $a = 100$  AU.

## Chapter 6

# Discussion

In this work, the effects of the passage of a star on the orbits of a planet were studied using a special case of the  $n$ -body problem called the hyperbolic restricted 3-body problem (HR3BP). An application of these changes were then studied, looking at how it could affect the climate on Earth.

One consideration to be made is the likelihood of a rogue star passing by the Solar System. Based on results from the Gaia telescope's second data release in April 2018, an estimated 694 stars will possibly approach our Solar System to less than  $1.543 \times 10^{14}$  km ( $1.0315 \times 10^6$  AU) in the next 15 million years. Of these, 26 have a greater than 50 % chance of coming within  $3.12 \times 10^{13}$  km (209000 AU) and another 7 within  $1.51 \times 10^{13}$  km (101000 AU) [2]. This number is likely much higher, due to the sheer number of stars needed to be surveyed. The present rate of encounters within 206564 AU (1 parsec) is estimated to be  $19.7 \pm 2.2$  per million years, a quantity expected to scale quadratically with the encounter distance out to at least several parsecs [2].

The first part of this work focuses on the star passing within 50 AU of the Sun in the Kuiper Belt. This distance is close enough to have an effect on Earth stronger than that of Jupiter. This means that not only will the changes to Jupiter's orbit exist, these



will compound with the changes to Earth's orbit from the star. This effect was observed to be dramatic enough that such a passage this close could be ruled out. An event such as this would be easily spotted in the geological record and as no such effect has been spotted, the conclusion stands that it probably did not occur. Indeed the number of stars passing within the outer regions of the Kuiper Belt (50 AU) during the life of the solar system is 0.0003, a highly unlikely occurrence.

In the second part of this work, the focus was on the sensitivity of the planetary orbits to the star's distance. The goal was to find where it is that minute changes are still perceptible as the star moves out towards the Oort Cloud. The effects of the passing star diminish as the star moves farther and farther away and the effects are unlikely to be spotted. The number of stars passing within the outer reaches of the Oort Cloud (50,000 AU) during the last 65 million years is about 75 and during the last 250 million years is about 289. The number of stars passing within the inner reaches of the Oort Cloud (3000 AU) during the last 250 million years is about 1. Over the life of the Solar System, which is approximately 4.568 billion years old, this would be about 19 stars [5]. While there is a much higher probability that a star passed within this region of the Solar System, the effects of the star would be negligible and difficult to perceive.

The results of this work, in addition to the cited survey of nearby stars, indicate that it is unlikely that one of these stars passed close enough to the Solar System that its effects would appear in the Earth's geological record. There does remain the distinct possibility that a rogue star did pass near enough to do so. Other interstellar objects have passed along hyperbolic orbits within the Solar System, making it more likely that a larger object could follow a similar path [53].

## 6.1 Future Work

From the results found here, more work is indicated on this question. There are several directions that one can explore based on these results. One immediate extension that arises is the expansion to the 3-dimensional case. The full 3-dimensional problem should be considered to see what happens when the star approaches from out of the plane could have effects on the obliquity, a Milankovitch cycle whose changes would have strong climatic effects. Another immediate improvement in the study could be made by studying the effects of some parameters that were held constant here. In this study, both the eccentricity of the passing star's orbit and its mass were held constant. The eccentricity of the passing star's orbit will change how close the rogue star would be to the planetary system. Additionally, rogue stars are stars that are roaming across the galaxy and therefore could be of any mass. One future study should focus on the effects that the mass of the star have on the distance of perceivable changes to the orbits of the planets in the Solar System.

# References

- [1] E. P. AKSENOV, *Averaged, restricted, circular three-body problem (averaged restricted circular three body problem, analyzing small mass motion about two bodies revolving about each other in circular orbits)*, Universitet Druzhby Narodov, Trudy, 21 (1967), pp. 184–202.
- [2] C. A. L. BAILER-JONES, J. RYBIZKI, R. ANDRAE, AND M. FOUESNEAU, *New stellar encounters discovered in the second gaia data release*, Astronomy & Astrophysics, 616 (2018), p. A37.
- [3] A. BERGER, M. LOUTRE, AND J. L. MÉLICE, *Equatorial insolation: from precession harmonics to eccentricity frequencies*, Climate of the Past, European Geosciences Union (EGU), 2 (2006), pp. 131–136.
- [4] V. V. BOBYLEV, *Searching for stars closely encountering with the solar system*, Astronomy Letters, 36 (2010), pp. 220 – 226.
- [5] A. BOUVIER AND M. WADHWA, *The age of the Solar System redefined by the oldest Pb–Pb age of a meteoritic inclusion*, Nature Geoscience, 3 (2010), pp. 637–641.
- [6] M. I. BUDYKO, *The effect of solar radiation variations on the climate of the earth*, Tellus, 21 (1969), pp. 611–619.

- [7] P. CHÛLEK AND J. A. COAKLEY, *Analytical analysis of a budyko-type climate model*, *Journal of the Atmospheric Sciences*, 32 (1975), pp. 675–679.
- [8] J. M. CORS AND J. LLIBRE, *Chaos in the hyperbolic restricted 3-body problem*, in *From Newton to Chaos*, Springer, 1995, pp. 315–318.
- [9] ———, *The global flow of the hyperbolic restricted three-body problem*, *Archive for rational mechanics and analysis*, 131 (1995), pp. 335–358.
- [10] ———, *Qualitative study of the hyperbolic collision restricted three-body problem*, *Nonlinearity*, 9 (1996), p. 1299.
- [11] T. J. CROWLEY AND K. KIM, *Milankovitch forcing of the last interglacial sea level*, *Science*, 265 (1994), pp. 1566–1568.
- [12] ———, *Comparison of longterm greenhouse projections with the geologic record*, *Geophysical Research Letters*, 22 (1995), pp. 933–936.
- [13] ———, *Comparison of proxy records of climate change and solar forcing*, *Geophysical Research Letters*, 23 (1996), pp. 359–362.
- [14] ———, *Modeling the temperature response to forced climate change over the last six centuries*, *Geophysical Research Letters*, 26 (1999), pp. 1901–1904.
- [15] T. J. CROWLEY, K. KIM, J. G. MENGEL, AND D. A. SHORT, *Modeling 100,000-year climate fluctuations in pre-pleistocene time series*, *Science*, 255 (1992), pp. 705–707.
- [16] T. J. CROWLEY, D. A. SHORT, J. G. MENGEL, AND G. R. NORTH, *Role of seasonality in the evolution of climate during the last 100 million years*, *Science*, 231 (1986), pp. 579–584.

- [17] M. DE SANCTIS, M. CAPRIA, AND A. CORADINI, *Thermal evolution and differentiation of edgeworth-kuiper belt objects*, *The Astronomical Journal*, 121 (2001), p. 2792.
- [18] G. N. DUBOSHIN, *Celestial mechanics: Basic problems and methods*, Izdatel'stvo Nauka, 1975.
- [19] A. S. DYKE, J. T. ANDREWS, P. U. CLARK, J. H. ENGLAND, G. H. MILLER, J. SHAW, AND J. J. VEILLETTE, *The laurentide and innuitian ice sheets during the last glacial maximum*, *Quaternary Science Reviews*, 21 (2002), pp. 9–31.
- [20] S. EPSTEIN, R. BUCHSBAUM, H. A. LOWENSTAM, AND H. C. UREY, *Revised carbonate-water isotopic temperature scale*, *Geological Society of America Bulletin*, 64 (1953), pp. 1315–1326.
- [21] M. B. FAINTICH, *Application of the restricted hyperbolic three-body problem to a star-sun-comet system*, *Celestial mechanics*, 6 (1972), pp. 22–26.
- [22] R. FITZPATRICK, *An Introduction to Celestial Mechanics*, Cambridge University Press, 2012.
- [23] J. D. HAYS, J. IMBRIE, AND N. J. SHACKLETON, *Variations in the earth's orbit: pacemaker of the ice ages*, *science*, 194 (1976), pp. 1121–1132.
- [24] H. KAPER AND H. ENGLER, *Mathematics and climate*, vol. 131, Siam, 2013.
- [25] J. KEPLER, *Astronomia Nova*, Green Lion Press, 1609. Translated by W.H. Donahue (2015).
- [26] ———, *Harmonice Mundi*, vol. 6 of *Gesammelte Werke*, 1619. reprinted (1837).
- [27] P. KERVILLA, F. THÉVENIN, D. SÉGRANSAN, G. BERTHOMIEU, B. LOPEZ, P. MOREL, AND J. PROVOST, *The diameters of  $\alpha$  centauri a and b—a comparison*

- of the asteroseismic and vinci/ulti views*, *Astronomy & Astrophysics*, 404 (2003), pp. 1087–1097.
- [28] P. KUSTAANHEIMO AND E. L. STIEFEL, *Perturbation theory of kepler motion based on spinor regularization*, *Journal für die Reine und Angewandte Mathematik*, 218 (1965), pp. 204–219.
- [29] J. LASKAR, *The limits of earth orbital calculations for geological time-scale use*, *Philosophical Transactions of the Royal Society of London. Series A: Mathematical, Physical and Engineering Sciences*, 357 (1999), pp. 1735–1759.
- [30] ———, *Chaos in the solar system*, in *Annales Henri Poincaré*, vol. 4 (Supp. 2), Springer, 2003, pp. 693–705.
- [31] J. LASKAR, A. FIENGA, M. GASTINEAU, AND H. MANCHE, *La2010: a new orbital solution for the long-term motion of the earth*, *Astronomy & Astrophysics*, 532 (2011), p. A89.
- [32] J. LASKAR, P. ROBUTEL, F. JOUTEL, M. GASTINEAU, A. CORREIA, AND B. LEVRARD, *A long-term numerical solution for the insolation quantities of the earth*, *Astronomy & Astrophysics*, 428 (2004), pp. 261–285.
- [33] T. LEVI-CIVITA, *Sur la Régularisation du Problème des Trois Corps*, *Acta Math*, 42 (1920), pp. 99–144.
- [34] F.-P. LUIS AND P.-C. ERNESTO, *The symmetric elliptic and hyperbolic restricted 3-body problem on the unit circle*, *Journal of Geometry and Physics*, 99 (2016), pp. 28–41.

- [35] R. MCGEHEE AND C. LEHMAN, *A paleoclimate model of ice-albedo feedback forced by variations in earth's orbit*, SIAM Journal on Applied Dynamical Systems, 11 (2012), pp. 684–707.
- [36] R. MCGEHEE AND E. WIDIASIH, *A quadratic approximation to budyko's ice-albedo feedback model with ice line dynamics*, SIAM Journal on Applied Dynamical Systems, 13 (2014), pp. 518–536.
- [37] W. B. MCKINNON, D. PRIALNIK, S. A. STERN, AND A. CORADINI, *Structure and evolution of kuiper belt objects and dwarf planets*, The solar system beyond Neptune, 1 (2008), pp. 213–241.
- [38] A. NADEAU AND R. MCGEHEE, *A simple formula for a planet's mean annual insolation by latitude*, Icarus, 291 (2017), pp. 46–50.
- [39] E. NOETHER, *Invariante variationsprobleme*, Königlich Gesellschaft der Wissenschaften Göttingen Nachrichten Mathematik-physik Klasse, 2 (1918), pp. 235–267.
- [40] G. R. NORTH, *Theory of energy-balance climate models*, Journal of the Atmospheric Sciences, 32 (1975), pp. 2033–2043.
- [41] G. R. NORTH AND T. J. CROWLEY, *Application of a seasonal climate model to cenozoic glaciation*, Journal of the Geological Society, 142 (1985), pp. 475–482.
- [42] G. R. NORTH, J. G. MENGEL, AND D. A. SHORT, *Simple energy balance model resolving the seasons and the continents: Application to the astronomical theory of the ice ages*, Journal of Geophysical Research: Oceans, 88 (1983), pp. 6576–6586.
- [43] G. R. NORTH AND M. J. STEVENS, *Energy-balance climate models*, Cambridge University Press Cambridge, 2006.

- [44] P. E. OLSEN, J. LASKAR, D. V. KENT, S. T. KINNEY, D. J. REYNOLDS, J. SHA, AND J. H. WHITESIDE, *Mapping solar system chaos with the geological orrery*, Proceedings of the National Academy of Sciences, 116 (2019), pp. 10664–10673.
- [45] H. PÄLIKE, J. LASKAR, AND N. J. SHACKLETON, *Geologic constraints on the chaotic diffusion of the solar system*, Geology, 32 (2004), pp. 929–932.
- [46] H. POLLARD, *Mathematical Introduction to Celestial Mechanics*, Prentice-Hall Mathematics Series, Prentice-Hall, 1966.
- [47] W. SELLERS, *A global climatic model based on the energy balance of the earth-atmosphere system*, Journal of Applied Meteorology, 8 (1969), pp. 392–400.
- [48] D. A. SHORT, J. G. MENGEL, T. J. CROWLEY, W. T. HYDE, AND G. R. NORTH, *Filtering of milankovitch cycles by earth’s geography*, Quaternary Research, 35 (1991), pp. 157–173.
- [49] A. B. SOROKOVICH, *The Averaged Hyperbolic Restricted Three-Body Problem*, Soviet Astronomy, 26 (1982), pp. 721–726.
- [50] D. SOUAMI AND J. SOUCHAY, *The solar system’s invariable plane*, Astronomy & Astrophysics, 543 (2012), p. A133.
- [51] K. F. SUNDMAN, *Recherches sur le problème des trois corps*, Ex Officina Typographica Societatis Litterariae Fennicae, 1907.
- [52] K. F. SUNDMAN ET AL., *Mémoire sur le problème des trois corps*, Acta mathematica, 36 (1913), pp. 105–179.
- [53] D. E. TRILLING, M. MOMMERT, J. L. HORA, D. FARNOCCHIA, P. CHODAS, J. GIORGINI, H. A. SMITH, S. CAREY, C. M. LISSE, M. WERNER, ET AL., *Spitzer*



- observations of interstellar object 1i/‘oumuamua*, *The Astronomical Journal*, 156 (2018), p. 261.
- [54] K. K. TUNG, *Topics in mathematical modeling*, Princeton University Press Princeton, NJ, 2007.
- [55] J. WALSH, *Climate modeling in differential equations*, *The UMAP Journal*, 36 (2015), pp. 325 – 363.
- [56] E. WIDIASIH, *Dynamics of the budyko energy balance model*, *SIAM Journal on Applied Dynamical Systems*, 2 (2013), pp. 2068 – 2092.
- [57] P. WIEGERT AND S. TREMAINE, *The evolution of long-period comets*, *Icarus*, 137 (1999), pp. 84–121.
- [58] D. R. WILLIAMS, *Jupiter Fact Sheet*, 2018 (accessed June 09, 2020). <https://nssdc.gsfc.nasa.gov/planetary/factsheet/jupiterfact.html>.
- [59] ———, *Sun Fact Sheet*, 2018 (accessed May 17, 2020). <https://nssdc.gsfc.nasa.gov/planetary/factsheet/sunfact.html>.
- [60] ———, *Earth Fact Sheet*, 2019 (accessed May 17, 2020). <https://nssdc.gsfc.nasa.gov/planetary/factsheet/earthfact.html>.
- [61] ———, *Planetary Fact Sheet - Ratio to Earth Values*, 2019 (accessed May 17, 2020). [https://nssdc.gsfc.nasa.gov/planetary/factsheet/planet\\_table\\_ratio.html](https://nssdc.gsfc.nasa.gov/planetary/factsheet/planet_table_ratio.html).
- [62] A. WINTER, H. ISHIOROSHI, T. WATANABE, T. OBA, AND J. CHRISTY, *Caribbean sea surface temperatures: Two-to-three degrees cooler than present during the little ice age*, *Geophysical Research Letters*, 27 (2000), pp. 3365–3368.

- [63] A. WINTNER, *The analytical foundations of celestial mechanics*, Princeton, NJ, Princeton university press; London, H. Milford, Oxford university press, 1941., (1941).

# Appendix A

## Mathematica Code

Mathematica was used to create all images and generate all numbers in this document.

The code is given in the section below.

### A.1 Regularized HR3BP in 2D

```
ClearAll["Global`*"]
SetAttributes[MyExport, HoldAll];
MyExport[picture_, type_] := (SetDirectory[NotebookDirectory[]];
  Export[ToString[HoldForm[picture]] <> "." <> ToString[type], picture])

Laplace[{z1_, z2_, w1_, w2_},
  m1_] := {(z1^2 - z2^2) - 2*(z1*w2 - z2*w1) (z1*w2 + z2*w1)/m1, (2*z1*z2) +
  2*(z1*w2 - z2*w1) (z1*w1 - z2*w2)/m1}/(z1^2 + z2^2)

Eccentricity[{z1_, z2_, w1_, w2_}, m1_] := Module[{a, b},
  {a, b} = Laplace[{z1, z2, w1, w2}, m1];
```

```

Sqrt[a^2 + b^2]]
SemiMajorAxis[{z1_, z2_, w1_, w2_}, m1_] :=
  With[{e = Eccentricity[{z1, z2, w1, w2}, m1], L = 2*(z1*w2 - z2*w1)},
    L^2/(m1*(1 - e^2))]
PerihelionAngle[{z1_, z2_, w1_, w2_}, m1_] := Module[{a, b},
  {a, b} = Laplace[{z1, z2, w1, w2}, m1]; ArcTan[a, b]*180/Pi]
Period[{z1_, z2_, w1_, w2_}, m1_] :=
  With[{A = SemiMajorAxis[{z1, z2, w1, w2}, m1]}, 2*Pi*Sqrt[A^3/m1]]

```

(\*HYPERBOLIC ORBIT\*)

```

a = 1000/5.2;
e = 2;
R[H_] := a*(e*Cosh[H] - 1)
tau[H_] := Sqrt[(e + 1)/(e - 1)] Tanh[H/2]
cos[H_] := (1 - tau[H]^2)/(1 + tau[H]^2)
sin[H_] := 2*tau[H]/(1 + tau[H]^2)
X[H_] := R[H]*cos[H]
Y[H_] := R[H]*sin[H]

```

```

ParametricPlot[{X[H], Y[H]}, {H, -2, 2}]

```

```

F10 = m2*(x - X[H])/((x - X[H])^2 + (y - Y[H])^2)^1.5 -
  m2*X[H]/(X[H]^2 + Y[H]^2)^1.5 // Simplify;
F20 = m2*(y - Y[H])/((x - X[H])^2 + (y - Y[H])^2)^1.5 -
  m2*Y[H]/(X[H]^2 + Y[H]^2)^1.5 // Simplify;

```

```

F1 = F10 /. {m2 -> 0.3550700522909202, x -> 2 (z1[s]^2 - z2[s]^2),
  y -> 4*z1[s]*z2[s], H -> H[s]};
F2 = F20 /. {m2 -> 0.3550700522909202, x -> 2 (z1[s]^2 - z2[s]^2),
  y -> 4*z1[s]*z2[s], H -> H[s]};

m1 = 0.6449299477090799; (*kg*)
m2 = 1 - m1;
ode = {z1'[s] == w1[s]/2, z2'[s] == w2[s]/2,
  w1'[s] == h1[s]*z1[s] - 2*(z1[s]^2 + z2[s]^2)*(F1*z1[s] + F2*z2[s]),
  w2'[s] == h1[s]*z2[s] - 2*(z1[s]^2 + z2[s]^2)*(F2*z1[s] - F1*z2[s]),
  h1'[s] == -2*F1*(z1[s]*w1[s] - z2[s]*w2[s]) -
  2*F2*(z1[s]*w2[s] + z2[s]*w1[s]),
  H'[s] == 2*(z1[s]^2 + z2[s]^2)/(e*Cosh[H[s]] - 1)};

(* JUPITER ORBIT *)
smax = 500;
For[i = 0, i < 100, i++,
  aJ = 1;
  eJ = 0.0489;
  z1j = 1/Sqrt[2] Sqrt[aJ (1 + eJ)]*Cos[Pi*i/100]; (*Sqrt[m1/(4*aJ)]*)

  z2j = 1/Sqrt[2] Sqrt[aJ (1 - eJ)]*Sin[Pi*i/100];
  w1j = -(1/Sqrt[2]) Sqrt[aJ (1 + eJ)] Sqrt[m1/aJ]*Sin[Pi*i/100];
  w2j = 1/Sqrt[2] Sqrt[aJ (1 - eJ)] Sqrt[m1/aJ] Cos[Pi*i/100];

```

```

h1j = (w1j^2 + w2j^2 - m1)/(2*(z1j^2 + z2j^2));
H0j = -3;
icj = {z1[-smax] == z1j, z2[-smax] == z2j, w1[-smax] == w1j,
      w2[-smax] == w2j, h1[-smax] == h1j, H[-smax] == H0j};

solj = NDSolve[
  ode~Join~icj, {z1[s], z2[s], w1[s], w2[s], h1[s], H[s]}, {s, -smax,
    smax}][[1]];
finaleccjup =
  Eccentricity[{z1[s], z2[s], w1[s], w2[s]}, m1] /. solj /. s -> smax;
finalsmajup =
  SemiMajorAxis[{z1[s], z2[s], w1[s], w2[s]}, m1] /. solj /. s -> smax;
finallaplacejup =
  Laplace[{z1[s], z2[s], w1[s], w2[s]}, m1] /. solj /. s -> smax;
finalperijup =
  PerihelionAngle[{z1[s], z2[s], w1[s], w2[s]}, m1] /. solj /. s -> smax;

perturbedorbitjupiter =
  ParametricPlot[{2 (z1[s]^2 - z2[s]^2), 4*z1[s]*z2[s]} /.
    solj, {s, -smax, smax},
  AxesLabel -> {"q1", "q2"}, PlotStyle -> Gray];
starorbit =
  ParametricPlot[{X[H[s]], Y[H[s]]} /. solj, {s, -smax, smax},
  AxesLabel -> {"q1", "q2"}, PlotStyle -> Blue ];
icorbitjupiter =
  ParametricPlot[{2 ((1/Sqrt[2] Sqrt[aJ (1 + eJ)]*

```

```

Cos[Sqrt[m1/(4*aJ)]*s]^2 - (1/Sqrt[2] Sqrt[aJ (1 - eJ)]*
Sin[Sqrt[m1/(4*aJ)]*s]^2),
4*(1/Sqrt[2] Sqrt[aJ (1 + eJ)]*Cos[Sqrt[m1/(4*aJ)]*s])*(1/Sqrt[2] Sqrt[
aJ (1 - eJ)]*Sin[Sqrt[m1/(4*aJ)]*s])}, {s, 0, Pi/Sqrt[m1/(4*aJ)]},
AxesLabel -> {"q1", "q2"}, PlotStyle -> {Gray, Dashed}];

finalorbitjupiter =
ParametricPlot[{2 ((1/Sqrt[2] Sqrt[finalsmajup (1 + finaleccjup)]*
Cos[Sqrt[m1/(4*finalsmajup)]*s])^2 - (1/Sqrt[2] Sqrt[
finalsmajup (1 - finaleccjup)]*Sin[Sqrt[m1/(4*finalsmajup)]*s])^2),
4*(1/Sqrt[2] Sqrt[finalsmajup (1 + finaleccjup)]*
Cos[Sqrt[m1/(4*finalsmajup)]*s])*(1/Sqrt[2] Sqrt[
finalsmajup (1 - finaleccjup)]*Sin[Sqrt[m1/(4*finalsmajup)]*s])}, {s,
0, 50}, AxesLabel -> {"q1", "q2"}, PlotStyle -> {Red}];

jupiterorbit =
Show[finalorbitjupiter, icorbitjupiter,
TicksStyle -> {{Medium, Black}, {Medium, Black}},
AxesStyle -> {{Medium, Black}, {Medium, Black}}];

jupandstar =
Show[starorbit, perturbedorbitjupiter, PlotRange -> {{-10, 10}, {-20, 20}},
AxesOrigin -> {0, 0}];

eccicjupiter =
Plot[Eccentricity[{1/Sqrt[2] Sqrt[aJ (1 + eJ)]*
Cos[Sqrt[m1/(4*aJ)]*s], 1/Sqrt[2] Sqrt[aJ (1 - eJ)]*
Sin[Sqrt[m1/(4*aJ)]*s], -(1/Sqrt[2]) Sqrt[
aJ (1 + eJ)] Sqrt[m1/aJ]*Sin[Sqrt[m1/(4*aJ)]*s],

```

```

1/Sqrt[2] Sqrt[aJ (1 - eJ)] Sqrt[m1/aJ] Cos[Sqrt[m1/(4*aJ)]*s]},
m1], {s, -smax, smax}, PlotRange -> All, AxesLabel -> {s, eccentricity},
PlotStyle -> {Gray, Dashed}];

eccorbjupiter =
Plot[Eccentricity[{z1[s], z2[s], w1[s], w2[s]}, m1] /. solj, {s, -smax,
smax}, PlotRange -> All, AxesLabel -> {s, eccentricity},
PlotStyle -> {Red}];

jupiterecc =
Show[eccicjupiter, eccorbjupiter, PlotRange -> {{-smax, smax}, {0, 0.1}},
AxesOrigin -> {0, 0}, TicksStyle -> {{Medium, Black}, {Medium, Black}},
AxesStyle -> {{Medium, Black}, {Medium, Black}}];

smaicjupiter =
Plot[SemiMajorAxis[{1/Sqrt[2] Sqrt[aJ (1 + eJ)]*
Cos[Sqrt[m1/(4*aJ)]*s], 1/Sqrt[2] Sqrt[aJ (1 - eJ)]*
Sin[Sqrt[m1/(4*aJ)]*s], -(1/Sqrt[2]) Sqrt[
aJ (1 + eJ)] Sqrt[m1/aJ]*Sin[Sqrt[m1/(4*aJ)]*s],
1/Sqrt[2] Sqrt[aJ (1 - eJ)] Sqrt[m1/aJ] Cos[Sqrt[m1/(4*aJ)]*s]},
m1], {s, -smax, smax}, PlotRange -> All, AxesLabel -> {s, semimajoraxis},
PlotStyle -> {Gray, Dashed}];

smaorbjupiter =
Plot[SemiMajorAxis[{z1[s], z2[s], w1[s], w2[s]}, m1] /. solj, {s, -smax,
smax}, PlotRange -> All, AxesLabel -> {s, semimajoraxis},
PlotStyle -> {Red}];

jupitersma =
Show[smaicjupiter, smaorbjupiter, PlotRange -> {{-smax, smax}, {0.5, 1.4}},

```



```

AxesOrigin -> {0, 0.5}, TicksStyle -> {{Medium, Black}, {Medium, Black}},
AxesStyle -> {{Medium, Black}, {Medium, Black}}];

```

```
laplaceicjupiter =
```

```

Plot[Laplace[{1/Sqrt[2] Sqrt[aJ (1 + eJ)]*
Cos[Sqrt[m1/(4*aJ)]*s], 1/Sqrt[2] Sqrt[aJ (1 - eJ)]*
Sin[Sqrt[m1/(4*aJ)]*s], -(1/Sqrt[2]) Sqrt[
aJ (1 + eJ)] Sqrt[m1/aJ]*Sin[Sqrt[m1/(4*aJ)]*s],
1/Sqrt[2] Sqrt[aJ (1 - eJ)] Sqrt[m1/aJ] Cos[Sqrt[m1/(4*aJ)]*s]},
m1], {s, -smax, smax}, PlotRange -> All,
AxesLabel -> {"s", "laplace vector"}, PlotStyle -> {Gray, Dashed}];

```

```
laplaceorbjupiter =
```

```

Plot[Laplace[{z1[s], z2[s], w1[s], w2[s]}, m1] /. solj, {s, -smax, smax},
PlotRange -> All, AxesLabel -> {"s", "laplace vector"}, PlotStyle -> {Red}];

```

```
jupiterlaplace =
```

```

Show[laplaceicjupiter, laplaceorbjupiter, PlotRange -> All,
AxesOrigin -> {0, 0}, TicksStyle -> {{Medium, Black}, {Medium, Black}},
AxesStyle -> {{Medium, Black}, {Medium, Black}}];

```

```
periicjupiter =
```

```

Plot[PerihelionAngle[{1/Sqrt[2] Sqrt[aJ (1 + eJ)]*Cos[Sqrt[m1/(4*aJ)]*s],
1/Sqrt[2] Sqrt[aJ (1 - eJ)]*Sin[Sqrt[m1/(4*aJ)]*s], -(1/Sqrt[2]) Sqrt[
aJ (1 + eJ)] Sqrt[m1/aJ]*Sin[Sqrt[m1/(4*aJ)]*s],
1/Sqrt[2] Sqrt[aJ (1 - eJ)] Sqrt[m1/aJ] Cos[Sqrt[m1/(4*aJ)]*s]},
m1], {s, -smax, smax}, PlotRange -> All,
AxesLabel -> {"s", "perihelion angle"}, PlotStyle -> {Gray, Dashed}];

```

```

periorbjupiter =
  Plot[PerihelionAngle[{z1[s], z2[s], w1[s], w2[s]}, m1] /. solj, {s, -smax,
    smax}, PlotRange -> All, AxesLabel -> {"s", "perihelion angle"},
    PlotStyle -> {Red}];
jupiterperi =
  Show[periicjupiter, periorbjupiter, PlotRange -> All, AxesOrigin -> {0, 0},
    TicksStyle -> {{Medium, Black}, {Medium, Black}},
    AxesStyle -> {{Medium, Black}, {Medium, Black}}];

Print["i = ", i, " ", "(", 2 (z1j^2 - z2j^2), " ", " ", 4*z1j*z2j, " ) ",
  " ecc=", finaleccjup, " %sma=", (finalsmajup - aJ)/aJ, " perihelion=",
  finalperijup]]

(* EARTH ORBITS *)
smax=500;
For[i = 0, i <16, i++,
  aE = 0.192;
  eE = 0.0167;
  z1e=1/Sqrt[2] Sqrt[aE (1+eE)]*Cos[Pi*i/16]; (*Sqrt[m1/(4*aJ)]*)
  z2e=1/Sqrt[2] Sqrt[aE (1-eE)]*Sin[Pi*i/16];
  w1e=-(1/Sqrt[2]) Sqrt[aE (1+eE)]Sqrt[m1/aE]*Sin[Pi*i/16];
  w2e=1/Sqrt[2] Sqrt[aE (1-eE)]Sqrt[m1/aE]Cos[Pi*i/16];
  h1e = (w1e^2+w2e^2-m1)/(2*(z1e^2+z2e^2));
  H0e=-3;
  ice = {z1[-smax]==z1e,z2[-smax]==z2e,w1[-smax]==w1e,

```

```

w2[-smax]==w2e,h1[-smax]==h1e,H[-smax]==H0e};

sole =NDSolve[ode~Join~ice,{z1[s],z2[s],w1[s],w2[s],h1[s],H[s]},
  {s,-smax,smax}][[1]];
finaleccearth=Eccentricity[{z1[s],z2[s],w1[s],w2[s]},m1]/.sole
  /.s->smax;
finalsmaearth=SemiMajorAxis[{z1[s],z2[s],w1[s],w2[s]},m1]/.sole
  /.s->smax;
finallaplacearth = Laplace[{z1[s],z2[s],w1[s],w2[s]},m1]/.sole
  /.s->smax;
finalperiearth = PerihelionAngle[{z1[s],z2[s],w1[s],w2[s]},m1]/.sole
  /.s->smax;

perturbedorbitearth=
ParametricPlot[{2(z1[s]^2-z2[s]^2),4*z1[s]*z2[s]}/.sole,{s,-smax,smax},
AxesLabel -> {x1[s], x2[s]}, PlotStyle -> Gray];
icorbitearth = ParametricPlot[{2((1/Sqrt[2] Sqrt[aE (1+eE)]*
  Cos[Sqrt[m1/(4*aE)]*s])^2 - (1/Sqrt[2] Sqrt[aE (1-eE)]*
  Sin[Sqrt[m1/(4*aE)]*s])^2),
  4*(1/Sqrt[2] Sqrt[aE (1+eE)]*Cos[Sqrt[m1/(4*aE)]*s])*(1/Sqrt[2]
  Sqrt[aE (1-eE)]*Sin[Sqrt[m1/(4*aE)]*s])}, {s, 0,Pi/Sqrt[m1/(4*aJ)]},
  AxesLabel -> {"Subscript[q, 1]", "Subscript[q, 2]"},
  PlotStyle -> {Gray,Dashed}];
finalorbitearth =
  ParametricPlot[{2((1/Sqrt[2] Sqrt[finalsmaearth(1+finaleccearth)]*
  Cos[Sqrt[m1/(4*finalsmaearth)]*s])^2 - (1/Sqrt[2]

```

```

Sqrt[finalsmaearth (1-finaleccearth)]*
Sin[Sqrt[m1/(4*finalsmaearth)]*s]^2),
4*(1/Sqrt[2] Sqrt[finalsmaearth(1+finaleccearth)]*C
os[Sqrt[m1/(4*finalsmaearth)]*s])*(1/Sqrt[2]
Sqrt[finalsmaearth (1-finaleccearth)]*
Sin[Sqrt[m1/(4*finalsmaearth)]*s]}},
{s, 0,50}, AxesLabel -> {"q1", "q2"},
PlotStyle -> {Darker[Green]}}];

earthorbit=Show[icorbitearth, finalorbitearth,
TicksStyle->{{Medium,Black}, {Medium, Black}}, AxesStyle->
{{Medium, Black}, {Medium, Black}}];

eccicearth = Plot[Eccentricity[{1/Sqrt[2] Sqrt[aE(1+eE)]*
Cos[Sqrt[m1/(4*aE)]*s],1/Sqrt[2] Sqrt[aE (1-eE)]*
Sin[Sqrt[m1/(4*aE)]*s],-(1/Sqrt[2]) Sqrt[aE
(1+eE)]Sqrt[m1/aE]*Sin[Sqrt[m1/(4*aE)]*s],1/Sqrt[2] Sqrt[aE
(1-eE)]Sqrt[m1/aE]Cos[Sqrt[m1/(4*aE)]*s]},m1],{s,-smax,smax},
PlotRange->All, AxesLabel -> {s, eccentricity}, PlotStyle -> {Gray, Dashed}];

eccorbearth =
Plot[Eccentricity[{z1[s],z2[s],w1[s],w2[s]},m1]/.sole,{s,-smax,smax},
PlotRange->All, AxesLabel -> {s, eccentricity},
PlotStyle -> {Darker[Green]}}];

earthecc=Show[eccicearth,eccorbearth, PlotRange -> {{-smax,smax},{0.01,0.025}},
AxesOrigin -> {0,0.01}, TicksStyle->{{Medium,Black}, {Medium, Black}},
AxesStyle-> {{Medium, Black}, {Medium, Black}}];

```

```

smaicearth = Plot[SemiMajorAxis[{1/Sqrt[2] Sqrt[aE(1+eE)]*
  Cos[Sqrt[m1/(4*aE)]*s],1/Sqrt[2] Sqrt[aE (1-eE)]*
  Sin[Sqrt[m1/(4*aE)]*s],-(1/Sqrt[2]) Sqrt[aE
  (1+eE)]Sqrt[m1/aE]*Sin[Sqrt[m1/(4*aE)]*s],1/Sqrt[2] Sqrt[aE
  (1-eE)]Sqrt[m1/aE]Cos[Sqrt[m1/(4*aE)]*s]},m1],{s,-smax,smax},
  PlotRange->All, AxesLabel -> {s, semimajoraxis},
  PlotStyle -> {Gray, Dashed}];

smaorbearth =
  Plot[SemiMajorAxis[{z1[s],z2[s],w1[s],w2[s]},m1]/.sole,{s,-smax,smax},
  PlotRange->All, AxesLabel -> {s, semimajoraxis},
  PlotStyle -> {Darker[Green]}}];

earth sma=Show[smaorbearth,smaicearth, PlotRange ->{{-smax,smax},{0,0.3}},
  AxesOrigin -> {0,0}, TicksStyle->{{Medium,Black}, {Medium, Black}},
  AxesStyle-> {{Medium, Black}, {Medium, Black}}];

laplaceicearth = Plot[Laplace[{1/Sqrt[2] Sqrt[aE(1+eE)]*
  Cos[Sqrt[m1/(4*aE)]*s],1/Sqrt[2] Sqrt[aE (1-eE)]*
  Sin[Sqrt[m1/(4*aE)]*s],-(1/Sqrt[2]) Sqrt[aE
  (1+eE)]Sqrt[m1/aE]*Sin[Sqrt[m1/(4*aE)]*s],1/Sqrt[2] Sqrt[aE
  (1-eE)]Sqrt[m1/aE]Cos[Sqrt[m1/(4*aE)]*s]},m11],{s,-smax,smax},
  PlotRange->All, AxesLabel -> {"s", "laplace vector"},
  PlotStyle -> {Gray, Dashed}];

laplaceorbearth = \
  Plot[Laplace[{z1[s],z2[s],w1[s],w2[s]},m1]/.sole,{s,-smax,smax},
  PlotRange->All, AxesLabel -> {"s", "laplace vector"},
  PlotStyle -> {Darker[Green]}}];

```

```

earthlaplace=Show[laplaceiceearth,laplaceorbearth, PlotRange -> All,
  AxesOrigin -> {0,0}, TicksStyle->{{Medium,Black}, {Medium, Black}},
  AxesStyle-> {{Medium, Black}, {Medium, Black}}];

periicearth = Plot[PerihelionAngle[{1/Sqrt[2]Sqrt[aE(1+eE)]*
  Cos[Sqrt[m1/(4*aE)]*s],1/Sqrt[2] Sqrt[aE(1-eE)]*
  Sin[Sqrt[m1/(4*aE)]*s],-(1/Sqrt[2]) Sqrt[aE
  (1+eE)]Sqrt[m1/aE]*Sin[Sqrt[m1/(4*aE)]*s],1/Sqrt[2] Sqrt[aE
  (1-eE)]Sqrt[m1/aE]Cos[Sqrt[m1/(4*aE)]*s]},m1],{s,-smax,smax},
  PlotRange->All, AxesLabel -> {"s", "perihelion angle"},
  PlotStyle -> {Gray, Dashed}];

periorbearth =
  Plot[PerihelionAngle[{z1[s],z2[s],w1[s],w2[s]},m1]/.sole,
  {s,-smax,smax}, PlotRange->All, AxesLabel -> {"s", "perihelion angle"},
  PlotStyle -> {Darker[Green]}];

earthperi=Show[periicearth,periorbearth, PlotRange -> All,
  AxesOrigin -> {0,0}, TicksStyle->{{Medium,Black}, {Medium, Black}},
  AxesStyle-> {{Medium, Black}, {Medium, Black}}];

Print["i = ", i, " ", "(" , 2(z1e^2-z2e^2), " , " , 4*z1e*z2e,") " ,
  earthorbit, " ", finaleccearth, earthecc, finalsmearth,
  earthsma, finalperiearth, earthperi ]]

```

## A.2 Budyko-Widiasih Model

```

Clear["Global`*"]
SetAttributes[MyExport, HoldAll];
MyExport[picture_, type_] := (SetDirectory[NotebookDirectory[]];
  Export[ToString[HoldForm[picture]] <> "." <> ToString[type],
    picture])

Q[a_, e_] = 342.998*a^2/Sqrt[1 - e^2];
beta = (23.5/180)*Pi;
sapprox[y_] =
  1 - (5/8)*LegendreP[2, Cos[beta]]*LegendreP[2, y] - (9/64)*
    LegendreP[4, Cos[beta]]*LegendreP[4, y] - (65/1024)*
    LegendreP[6, Cos[beta]]*LegendreP[6, y];
Integrate[sapprox[y], {y, 0, 1}];
sapproxplot =
  Plot[sapprox[y], {y, 0, 1}, PlotStyle -> Black, AspectRatio -> 1,
    AxesLabel -> {"sin(lat)", "Insolation"}];
sigma[y_, gamma_] :=
  Sqrt[1 - (Sqrt[1 - y^2] * Sin[beta] * Cos[gamma] -
    y * Cos[beta])^2];
s[y_] := (2/Pi^2) *
  NIntegrate[sigma[y, gamma], {gamma, 0, 2 * Pi}];
sfirstprincplot =
  Plot[s[y], {y, 0, 1}, PlotStyle -> {Black, Dashed},
    AspectRatio -> 1, AxesLabel -> {"sin(lat)", "Insolation"}];
Show[sfirstprincplot, sapproxplot]

```

```

alpha1 = 0.32; (*land/water*)
alpha2 = 0.62; (*ice*)
alpha[eta_, y_] :=
  Piecewise[{{Subscript[alpha, 1],
    0 <= y < eta}, {Subscript[alpha,
    2], eta < y <=
    1}, {(Subscript[alpha, 1] + Subscript[alpha, 2])/2,
    y == eta}}]
Manipulate[
  Plot[alpha[eta, y], {y, 0, 1}, AspectRatio -> 1,
    AxesLabel -> Automatic, PlotStyle -> Black], {eta, 0,
  1}]

A = 202;
B = 1.9;
o[T_] := A + B*T
Plot[o[T], {T, 250, 300}, PlotStyle -> {Black}, AspectRatio -> 1,
  AxesLabel -> {"T", "OLR"}]

alphabar2[eta_] :=
  NIntegrate[Subscript[alpha, 1]*sapprox[y], {y, 0, eta}] +
  NIntegrate[Subscript[alpha, 2]*sapprox[y], {y, eta, 1}];

```



```

alphabar[eta_] =
  0.62 (1. - 1.2187411549050502 eta +
    0.1644023830328752 eta^3 + 0.07139427615677992 eta^5 -
    0.017055504284604825 eta^7) +
  0.32 (0. + 1.2187411549050502 eta -
    0.1644023830328752 eta^3 - 0.07139427615677992 eta^5 +
    0.017055504284604825 eta^7);
Tbarstar[eta_, a_, e_] := (Q[a, e]*(1 - alphabar[eta]) - A)/
  B; (*This represents the Global Mean Temperature *)
c = 3.04;
Plot[Tbarstar[eta, 1, 0.0167] ], {eta, 0, 1}, PlotStyle -> Black,
  AxesLabel -> {"eta", "GMT"},
  TicksStyle -> {{Medium, Black}, {Medium, Black}},
  AxesStyle -> {{Medium, Black}, {Medium, Black}},
  AxesOrigin -> {0, 0}]

Tstar[eta_, y_, a_,
  e_] := (Q[a, e]*sapprox[y] (1 - alpha[eta, y]) - A +
  c*Tbarstar[eta, a, e])/(B + c);
Plot[Tstar[Sin[66.5*Pi/180], y, 1, 0.0167], {y,
  0, 1}, PlotStyle -> {Black, Thick}]

```